The uncertain future of mountaintop-removal-mined landscapes 2: Modeling the influence of topography and vegetation

Samuel J. Bower[a], Charles M. Shobe[a,b], Aaron E. Maxwell[a], Benjamin Campforts[c]

[a]*Department of Geology and Geography, West Virginia University, Morgantown, WV, USA*
[b]*Now at: United States Forest Service, Rocky Mountain Research Station, Fort Collins, CO, USA*
[c]*Department of Earth Sciences, Vrije University, Amsterdam, Netherlands*

SJB: sjb00020@mix.wvu.edu

CMS: charles.shobe@usda.gov (corresponding author)

AEM: aaron.maxwell@mail.wvu.edu

BC: b.campforts@vu.nl

Graphical Abstract

The uncertain future of mountaintop-removal-mined landscapes 2: Modeling the influence of topography and vegetation

Samuel J. Bower, Charles M. Shobe, Aaron E. Maxwell, Benjamin Campforts

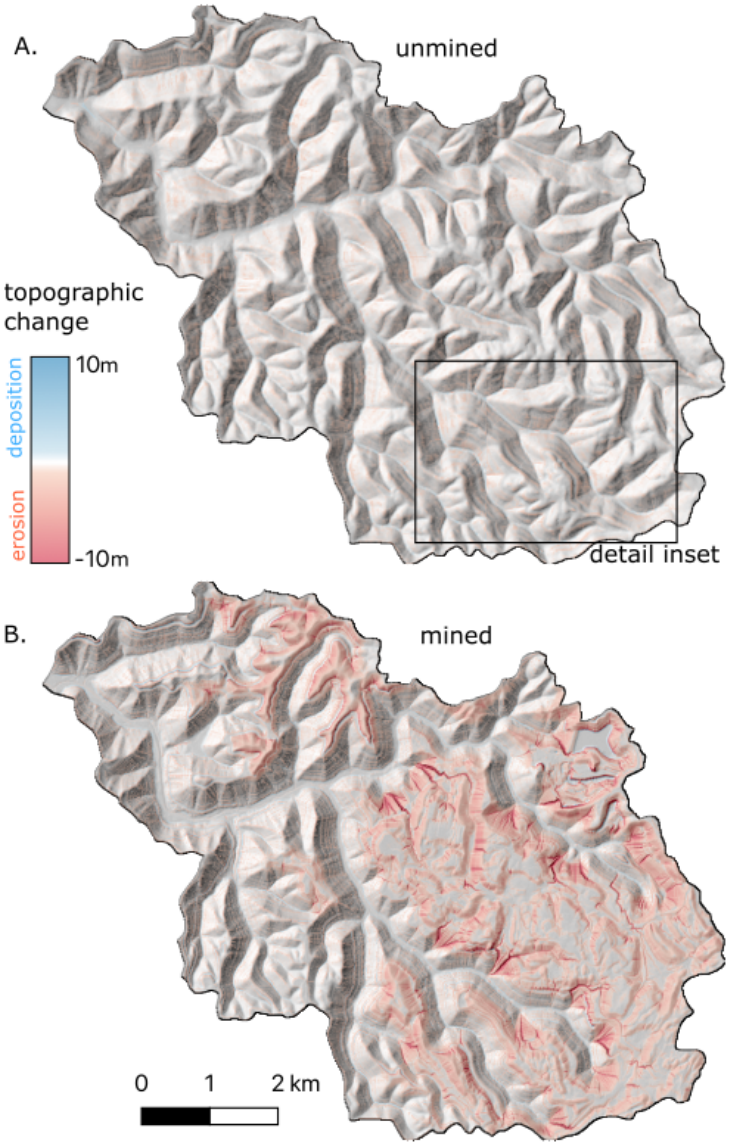

Highlights

The uncertain future of mountaintop-removal-mined landscapes 2: Modeling the influence of topography and vegetation

Samuel J. Bower, Charles M. Shobe, Aaron E. Maxwell, Benjamin Campforts

- We model 10,000 years of erosion beginning from both pre- and post-mining topography.
- Topographic alterations alone reduce total erosion due to ridge flattening.
- Incomplete vegetation recovery increases erosion in mined over unmined basins.
- Erosion is focused in valley fills, deposition in low-order valleys and below scarps.
- Vegetation recovery sets decadal sediment pulses and millennial landscape trajectory.

The uncertain future of mountaintop-removal-mined landscapes 2: Modeling the influence of topography and vegetation

Samuel J. Bower[a], Charles M. Shobe[a,b,*], Aaron E. Maxwell[a], Benjamin Campforts[c]

[a]*Department of Geology and Geography, West Virginia University, Morgantown, WV, USA*
[b]*Now at: United States Forest Service, Rocky Mountain Research Station, Fort Collins, CO, USA*
[c]*Department of Earth Sciences, Vrije University, Amsterdam, Netherlands*

Abstract

Erosion following human disturbance threatens ecosystem health and inhibits effective land use. Mountaintop removal (MTR) mined landscapes of the Appalachian Coalfields region, USA, provide a unique opportunity to quantify the geomorphic trajectory of disturbed lands. Here we assess how MTR-induced changes to topography and vegetation influence spatiotemporal erosion patterns by modeling landscape evolution in five mined watersheds. We use landscape evolution models starting from pre-MTR and post-MTR topographic data to isolate the influence of mining-induced topographic change. We then constrain ranges of erodibility from incision depths of gully features on mine margins, and use those estimates to model the influence of vegetation recovery trends on erosion.

Results show that topographic alterations alone reduce total sediment flux from mined catchments. Model runs that incorporate the disturbance and recovery of vegetation in mined watersheds show that, in any scenario other than complete vegetation recovery, vegetation disturbance drives higher total sediment export from mined catchments than from unmined catchments. Scenarios with no vegetation disturbance or full recovery exhibit sediment fluxes that decline over time post-recovery, while those without full recovery experience fluxes that increase over time even after recovery is complete. Spatiotemporal erosion trends depend on 1) the extent of vegetation recovery and 2) the extent to which MTR has created slope–area disequilib-

*charles.shobe@usda.gov

rium in the landscape. Valley fills, headwater valleys that have been filled with waste rock, experience erosion rates orders of magnitude higher than those found in the unmined landscape, as do steep scarps left behind by mining. Rapid erosion of mined areas drives sediment accumulation in colluvial hollows, headwater stream valleys, and below mine scarps. Our numerical experiments suggest that reclamation practices focused on reducing hotspots of slope–area disequilibrium and controlling erosion during the first few decades of vegetation recovery would reduce the extent to which mined Appalachian watersheds experience different landscape evolution trajectories from unmined ones both during and long after the vegetation recovery period. Insights gained from MTR-influenced landscapes have the potential to improve mined land management as the renewable energy transition drives increased surface mining.

Keywords: Post-mining erosion, Landscape evolution, Appalachia, Reclamation, Erosion prediction

---

1. Introduction

Human-induced rates of earth-moving outpace natural rates by upwards of an order of magnitude (Hooke, 2000; Wilkinson, 2005). Understanding present and future dynamics of landscape evolution requires the study of Earth's surface as a couple natural-human system (Pelletier et al., 2015).

One of the most significant contributors to anthropogenic earth-moving and subsequent landscape change is surface mining—the extraction of material by stripping of overburden from above. Some of the highest rates of mass redistribution in the contiguous United States, for example, are found in the Appalachian Coalfields (AC) region (Hooke, 1999), despite relatively low geological erosion rates in this area (Portenga et al., 2019). This discrepancy is caused by widespread surface coal mining (e.g., Skousen and Zipper, 2021), a process of mass redistribution several orders of magnitude more efficient than background geologic processes (Hooke, 1999). The impending renewable energy transition promises to usher in a global acceleration in earth moving through surface mining due to increased demand for critical minerals (Vidal et al., 2013; Sonter et al., 2018; Sovacool et al., 2020; Shobe, 2022). Studying how post-mining landscapes evolve is therefore essential to minimizing geomorphological and environmental disturbances (e.g., Hancock et al., 2020a).

The AC region provides a particularly instructive case study in post-mining landscape change because of the sheer magnitude of topographic rearrangement driven by mountaintop removal (MTR) mining, a region-specific type of surface mining where, rather than bench cutting along contours, the entirety of the rock mass above a horizontal coal seam is blasted/scraped off (Skousen and Zipper, 2021). The resulting waste rock is packed and terraced in headwater valleys—resulting in landforms known as valley fills—to lower the risk of slope failure and prevent erosion. The resulting landscape is geomorphically novel in the sense that it contains configurations of landforms that would not develop through landscape self-organization (Reed and Kite, 2020; Jaeger and Ross, 2021). Because MTR landscapes are not self-formed, these unnatural landscapes are likely to experience unnatural trajectories of post-mining landscape evolution, leading to undesirable geomorphological and environmental outcomes. Developing the ability to predict how MTR-mined landscapes evolve once mining and reclamation are complete will allow improved protection of ecosystems and water resources, and will provide a useful case study that can be applied to improve management of mined lands globally.

Numerical forward modeling of landscape evolution provides a framework for predicting how mass redistribution will modify landscapes in the future (e.g., Tucker and Hancock, 2010; Barnhart et al., 2020b; Hancock and Willgoose, 2021; Kwang et al., 2023). Landscape evolution models have already enabled extensive geomorphic prediction and hypothesis testing in post-mining landscapes (e.g., Willgoose and Riley, 1998; Lowry et al., 2013; Hancock et al., 2000, 2015). While static, empirical soil erosion models (i.e., RUSLE) have been used to assess the short-term geomorphic effects of MTR mining (Sears et al., 2020), there have been no long-term process-based studies of the geomorphic response to MTR mining in the AC region.

In this study we seek to understand how post-MTR landscapes evolve and how their trajectories of landscape evolution differ from unmined AC landscapes. To do this we leverage a unique dataset consisting of pre- and post-mining digital elevation models (DEMs) of a portion of the AC region. MTR mining in the AC presents us with an unnatural experiment (cf. Tucker, 2009) that we can use to directly compare landscape evolution dynamics between unmined watersheds, which were captured in the pre-mining DEM but no longer exist, and mined watersheds. We explore two influences of MTR mining on subsequent landscape evolution: alterations to topography driven by mining-induced mass redistribution and changes to land-surface

erodibility caused by the loss, and potential subsequent recovery, of forest cover on mined lands. Our goals are to quantify:

1. Differences between pre- and post-mining landscape evolution driven by mining-induced topographic change alone, and
2. The sensitivity of post-mining landscape change to the extent of vegetation recovery.

The current study follows from our companion paper (Shobe et al., in review), which identifies how MTR mining changes geomorphic processes and variables. Here we quantify how those changes influence post-mining landscape evolution.

2. Background: Post-MTR landscape evolution

MTR mining leaves behind landscapes that are significantly altered from their natural state. Our companion paper (Shobe et al., in review) analyzes these modifications in detail; here we summarize the key changes induced by MTR that might influence future landscape change. MTR alters topography, land-surface hydrology, vegetation, and surface and subsurface material properties. These changes lead to erosion process dynamics that differ between mined and unmined landscapes.

MTR mining flattens ridgetops and fills headwater river valleys with waste rock, creating plateau-like landscapes that cover tens of square kilometers (Fig. 1). These effects are prevalent throughout the AC region; mined areas cover >5,900 km^2 of land area in the AC (Pericak et al., 2018) and valley fills have buried >2,000 km of headwater streams (Bernhardt and Palmer, 2011). The cutting and filling method of MTR causes meaningful alterations to drainage basin elevation, slope, and drainage area distributions (Maxwell and Strager, 2013; Ross et al., 2016; Jaeger and Ross, 2021; Shobe et al., in review). MTR mining creates large areas of the landscape with near-zero slopes where mountaintops have been removed, as well as new steeply sloping areas where valley fills in headwater valleys end and grade steeply down to the old valley bottom (Ross et al., 2016; Jaeger and Ross, 2021). Average catchment elevation, slope, and slope–area product are significantly, monotonically correlated with the percent of a catchment that has undergone MTR mining—positively, negatively, and negatively, respectively (Shobe et al., in review). The proportion of the landscape classified as steepland landforms declines in mined areas (Maxwell and Strager, 2013).

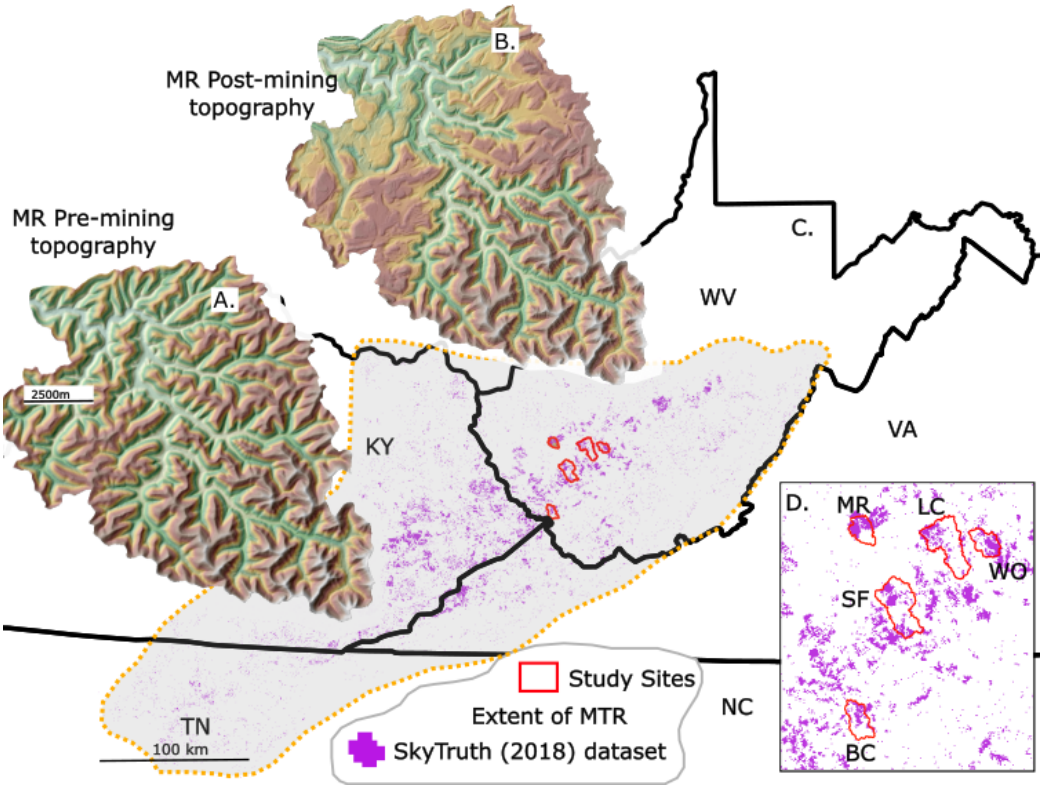

Figure 1: Study region overview. The extent of MTR is approximated by the grey polygon encompassing the purple regions, which are areas mapped as mined from 1985–2015 Landsat imagery (Pericak et al., 2018). Insets A and B show the pre-mining and post-mining DEMs of the Mud River watershed. Panel D zooms in to the five study watersheds. BC: Ben Creek, LC: Laurel Creek, MR: Mud River, SF: Spruce Fork, WO: White Oak.

The impact of MTR on surface and groundwater hydrology is complex due to variations among reclamation techniques and individual MTR landforms (Phillips, 2004; Miller and Zégre, 2014; Nippgen et al., 2017; Shobe et al., in review). Changes in topography (primarily slope reduction) and the de-vegetation of large portions of drainage basins influence surface hydrology, as do mining-induced changes to the water balance and flow routing. Across the mined landscape in general, infiltration rates tend to be lower than for unmined areas for the first few years post-mining (e.g., Guebert and Gardner, 2001). Cut surfaces—areas where mass has been removed—tend to have lower infiltration rates than filled areas, because in cut areas bedrock

is close to the surface while filled areas are underlain by tens of meters of well-fractured mine spoil. This duality accounts for field observations suggesting that though high volumes of runoff might be generated from the cut portions of mined landscapes (Negley and Eshleman, 2006) and drive local erosion hotspots (Reed and Kite, 2020), the larger-scale catchment hydrology of mined basins often shows higher baseflows and less stormflow than nearby unmined basins (Nippgen et al., 2017).

MTR causes changes to vegetation and subsequent recovery trends that create permanently altered ecological conditions. Reclamation regulations mandate post-mining planting, but do not require restoration to the original forested state—regulations allow landowners to select vegetation recovery plans to accommodate desired land use (Bell et al., 1989; Skousen and Zipper, 2014). Remote-sensing-derived indices of vegetation recovery indicate that mine sites that attempted reforestation have not in general experienced the return of mature forests. Proxies for vegetation recovery tend to, over the decades since reclamation, asymptotically approach values that are suboptimal relative to undisturbed ecosystems (Ross et al., 2021; Thomas et al., 2022). A reasonable rule of thumb for post-mining forest recovery, given the inherent complexity in succession dynamics and the limitation of remotely sensed vegetation proxies, is to say that it recovers towards the pre-mining condition but that it may never recover fully.

MTR also dramatically alters surface and subsurface material properties. Once mining ceases, the mined area is resurfaced with minesoil, which can be soil that is stockpiled from the pre-mining landscape, brought in from elsewhere, or constructed by crushing waste rock (Bell et al., 1989). Beneath the few cm to tens of cm of minesoil, there can exist intact bedrock (in cut areas) or deep piles of highly heterogeneous waste rock (filled areas). Both minesoils and the waste rock that can underlie them are highly heterogeneous. Minesoils often exhibit grain size distributions that are overall finer than native soils, but with a disproportionately large coarse fraction (Feng et al., 2019). Valley fill deposits typically have a framework of large boulders at the base overlain by highly variable sand- to boulder-sized fill (e.g., Greer et al., 2017). Though geotechnical properties of minesoils and underlying fill vary widely, mined landscapes likely have less near-surface cohesion than their natural counterparts due to the combination of vegetation loss and physical heterogeneity (Shobe et al., in review).

Changes to topography, hydrology, vegetation, and material properties cause unique erosion dynamics on post-MTR landscapes. Investigations of

slope-area relationship in mined watersheds show shifts towards fluvial erosion in portions of slope-area space where hillslope processes once dominated (Jaeger and Ross, 2021). These process changes manifest in mined landscapes as deeply incised gullies on the peripheries of mined areas (Reed and Kite, 2020).

While there are no studies forecasting how changes driven by MTR mining might integrate to influence post-MTR landscape evolution, we can draw general insights from other regions and types of mines. An extensive body of work centered around the evolution of spoil piles and other landforms on Australian Uranium mines has yielded insight into how mined landscape might evolve. In these settings, landscape evolution is dominated by rapid gully erosion that moves sediment quickly during and after mining (Hancock et al., 2000, 2015; Hancock and Willgoose, 2021). Modeling studies suggest that vegetation (Evans and Willgoose, 2000; Hancock et al., 2015; Lowry et al., 2019), precipitation (Hancock et al., 2017b,a; Lowry et al., 2019), and grain size (Lowry et al., 2019; Hancock et al., 2020b) all have significant impacts on sediment flux over annual timescales and catchment hypsometry over geologic timescales (Hancock et al., 2016). Most important in controlling the trajectory of landscape change is the shape of the post mining landscape, which governs the distribution of slope and drainage area across the landscape (e.g., Lowry et al., 2019; Hancock et al., 2020a; Jaeger and Ross, 2021).

In this study we seek to gain similar insight into the evolution of post-MTR landscapes. We model the effects of two of the four key modifications to post-MTR landscapes: topography and vegetation. Though we suspect that alterations to hydrology and surface material properties are also important (Shobe et al., in review), these influences are less well-quantified than changes to topography (revealed by DEMs) and vegetation (revealed by metrics like NDVI) (Maxwell and Strager, 2013; Ross et al., 2016, 2021; Thomas et al., 2022).

3. Methods

We seek to elucidate the influence of 1) topographic alteration and 2) vegetation (non-)recovery on post-MTR landscape evolution through numerical landscape evolution experiments using pre- and post-mining DEMs.

3.1. Experimental design

We model landscape evolution over the next 10 kyr for five heavily mined watersheds in the AC region. For each watershed, we conduct a control simulation in which landscape evolution begins from the pre-mining DEM and we assume no changes to geomorphic processes or variables. Control simulations reveal the trajectory of landscape change the watershed would have experienced had it not been mined or subjected to any other major disturbance.

To isolate the influence of MTR-driven topographic change, we conduct a simulation for each watershed using the post-mining DEM under the simplifying assumption that nothing has changed due to mining except the watershed's topography. We do not suggest that mined landscapes experience no other alterations (see Shobe et al., in review), only that comparing these results with the results of the unmined simulations allows us to isolate the influence of topographic change.

We then explore how the recovery, or lack thereof, of vegetation influences post-mining landscape evolution. We do this by manipulating the erodibility of the land surface under the assumption that more mature vegetation communities (i.e., forest) reduce erodibility by increasing soil cohesion. We simulate three vegetation recovery scenarios (Sec. 3.4.1) for each watershed: one scenario in which vegetation (and therefore erodibility) does not recover at all post-mining, one in which vegetation recovers to its pre-mining state, and one where vegetation recovery returns erodibility half of the way to its pre-mining value.

Our experimental design results in five forward models of landscape change in each study watershed: one based on the pre-mining topography, one in which only topography has been influenced by mining, and three exploring the sensitivity of post-mining landscape evolution to vegetation-related erodibility changes. We do not investigate changes to hydrology and material properties (e.g., Shobe et al., in review), in this initial analysis.

3.2. Study watersheds

This study uses five hydrologic unit code 12 (HUC-12) catchments from the AC region (Fig. 1). These watersheds are representative of mined watersheds in the AC in that they display high relief and steep hillslopes driven by river incision that outpaces lithologically controlled ridgetop lowering. We focus on these five watersheds because their pre- and post-mining geomorphology was quantified and characterized in detail by Jaeger and Ross

HUC-12 ID	Name	A [km^2]	Pre-R [m]	Post-R [m]	% mined
050702010302	Ben Creek	60	524	521	25
050500090602	Laurel Creek	130	478	458	22
050701020302	Mud River	50	280	280	38
050500090302	Spruce Fork	130	500	477	20
050500090601	White Oak	50	513	467	31

Table 1: The five study watersheds. A is catchment area, Pre-R is pre-mining topographic relief, and Post-R is post-mining topographic relief. Percent mined values are calculated from landsat-derived mining extents (Pericak et al., 2018).

(2021). Study watersheds range from 50 to 130 km^2 in area and have all experienced MTR mining over at least 20% of their surface area (Table 1); this has dramatically rearranged their topography (DEMs in Fig. 1). We note that because MTR rearranges drainage divides (Shobe et al., in review), watershed boundaries do not remain the same between the pre- and post- mining cases. Given that we have to keep our analysis area consistent, however, we use the HUC-12 watershed boundaries for both cases.

MTR mining has meaningfully changed the topography of all five catchments (Figs. 1 and 2; Jaeger and Ross (2021)). Mining has narrowed their elevation distributions as peaks are flattened and valleys are filled (Fig. 2A–E). Slope distributions become bimodal with increasing proportions of low slopes that represent flattened areas (Fig. 2F–J). Distributions of the slope-area product ($\sqrt{A}S$, a proxy for the efficacy of erosion by flowing water; Howard and Kerby (e.g., 1983)) show increasing proportions of the landscape underlain by areas of low $\sqrt{A}S$, both because slopes are reduced in general and because headwater valleys have been replaced with flat regions in which flow does not accumulate as efficiently with distance (Fig. 2K–O). Bayesian Wilcoxon signed-rank tests (van Doorn et al., 2020) comparing pre- and post-mining distributions suggest that all three topographic metrics are significantly different between the pre- and post-mining DEMs of all five watersheds. The pre- and post-MTR topography for each catchment will serve as initial conditions in the modeling study and allow for quantitative comparison of erosion of disturbed landscapes and their now-lost natural counterparts.

3.3. Numerical modeling approach

We model sediment erosion, transport, and deposition on pre- and post-mining DEMs over the next 10 kyr. Our modeling approach errs on the side of simplicity, attempting to incorporate environmental complexity where we have the data to do so while avoiding unconstrained complexity. This requires making major simplifications to the treatment of surface hydrology and landscape matieral properties, the implications of which we discuss in detail in Sec. 5.4.

To capture erosion by overland flow, we use the Stream Power with Alluvium Conservation and Entrainment (SPACE) model (Shobe et al., 2017) in the Landlab modeling toolkit (Barnhart et al., 2020a). Sediment transport by creep and heave processes is modeled using a linear diffusion equation (e.g., Culling, 1963).

The model treats elevation change over time $\frac{\partial z}{\partial t}$ [m/yr] as the sum of fluvial and hillslope processes:

$$\frac{\partial z}{\partial t} = U + \frac{D_s - E_s}{1 - \phi} + D\nabla^2 z, \tag{1}$$

where U [m/yr] is rock uplift relative to baselevel, D_s and E_s are volumetric rates per unit bed area of sediment deposition and entrainment [m/yr], respectively, ϕ is bed sediment porosity [-], and D is the efficiency of hillslope sediment transport [m^2/yr].

Our formulation excludes the bedrock erosion term commonly incorporated in the SPACE model, making it equivalent to the erosion–deposition model of Davy and Lague (2009). While we acknowledge that bedrock lies near the surface in portions of both unmined and mined AC landscapes, we do not have 1) adequate constraints on depth to bedrock across our study watersheds or 2) a way to establish reasonable bounds on bedrock erodibility. By neglecting bedrock erosion we are implicitly assuming that AC bedrock has similar erodibility to overlying sediment, which may or may not be true at any given location but is not an unreasonable starting assumption given the heterogeneity in both AC bedrock and in unmined and post-mining AC soils.

The volumetric sediment entrainment rate per unit bed area E_s is

$$E_s = K\left(x,t\right)\left(AP\right)^{0.5} S^n, \tag{2}$$

where $K(x,t)$ [$m^{-0.5}yr^{-0.5}$] is the erodibility of surface material which we vary as a parameter in space and time, A is drainage area [m^2], P is mean annual precipitation (MAP) [m/yr], S is surface slope, and n is a slope exponent. There is no limitation placed on entrainment rate by sediment (un-)availability (Shobe et al., 2017) because we do not distinguish between sediment and bedrock. Eq. 2 encapsulates our two most significant model simplifications: the assumption that erosion by flowing water is set by drainage area and MAP, and the assumption that both cut and filled portions of MTR landscapes exhibit similar material properties.

The volumetric sediment deposition rate per unit bed area D_s is

$$D_s = \frac{Q_s}{Q} V, \tag{3}$$

where Q_s is volumetric sediment flux [m^3/yr], Q is volumetric water discharge [m^3/yr] and V is the effective sediment settling velocity [m/yr].

We route flow using D8 routing with the Priority Flood algorithm (Barnes, 2017) which routes flow across depressions in the landscape. This is important on MTR landscapes where there are many flat regions and engineered depressions (Reed and Kite, 2020; Shobe et al., in review).

3.4. Constraining parameter values

The model contains several parameters, some of which we treat as steady and uniform and some of which are unsteady and/or nonuniform. Sediment porosity ϕ is fixed at 0.3 and the slope exponent n at 1. The efficiency of hillslope sediment transport D is treated as steady and uniform with a value of 0.003 m^2/yr, taken from a recent global compilation that includes the Appalachians (Richardson et al., 2019). A major assumption we make is that the efficiency of hillslope sediment transport does not vary between unmined and mined landscapes. While this is not likely to be strictly true given the differences in material properties between unmined and mined areas, erosion by flowing water is thought to be the dominant erosion mechanism on MTR landscapes (Reed and Kite, 2020; Jaeger and Ross, 2021). Further, given that our timescale of interest is only 10 kyr, the efficiency of hillslope transport is unlikely to exert a first-order control on landscape evolution (e.g., Barnhart et al., 2020b). So while we likely miss second-order details of the system by keeping hillslope transport efficiency constant, changes to AC hillslope processes driven by mining are probably not as important as changes to fluvial incision processes.

3.4.1. Fluvial erodibility and the influence of vegetation recovery

Gully incision by flowing water is thought to be the dominant agent of post-MTR landscape evolution (Reed and Kite, 2020; Jaeger and Ross, 2021), so quantitatively constraining the fluvial erodibility constant K is paramount. Erodibility depends on the revegetation trajectory of mined landscapes. Increased vegetation cover and root density on mined lands likely has a variety of erosion inhibiting effects (Shobe et al., in review) ranging from reducing overland flow volumes by increasing evapotranspiration (e.g., Nippgen et al., 2017) to increasing soil cohesion (e.g., Simon and Collison, 2002). We might therefore expect erodibility to be highest immediately post-reclamation when mines are planted with grasses or small saplings. Erodibility might then decrease over reforestation timescales as succession occurs. Though revegetation does occur to some extent, the consensus is that forests do not return to their pre-mining state over the multidecadal timescales for which we have observations (e.g., Wickham et al., 2013; Ross et al., 2021; Thomas et al., 2022).

We constrain the range of K on MTR-mined landscapes by mapping gullies from lidar data (Fig. 3) and using gully morphology and erosion rates to calculate K (Fig. 4). We assume, based on past field observations (Reed and Kite, 2020; Jaeger and Ross, 2021), that gullies on post-mine landforms are features that post-date mining because deeply incised gullies are not commonly observed in natural Appalachian landscapes. Constraining K by mapping erosional features allows us to assess the integrated effects of changes to surface material properties, vegetation, and the erosivity of overland flow (for example due to changes in storm hydrographs), influences which we do not have the data to tease apart individually.

Because our methodology relies on mapping post-mining erosion features to calculate K, it cannot produce estimates of K for unmined Appalachian landscapes. Geologic-timescale estimates of K for this region come from Gallen (2018), who used river profile analysis to find a region-averaged K value for the Appalachian Plateau of approximately 1.3×10^{-6} $\mathrm{m^{0.1}y^{-1}}$. We assume that this regional average value applies to unmined landscapes (and that a 0.05 difference in area exponent between Gallen (2018)'s analysis and ours is negligible). We then take the ratio between the median and minimum K values we infer from gullies on mined lands (Fig. 4) as representative of the extent to which mining can cause K to rise above its natural value. By doing so we implicitly assume that the lowest-erodibility post-mining land-

scapes have similar erodibilities to undisturbed landscapes. We do not have evidence for or against the validity of this assumption, but it is unavoidable because we do not have independent constraints from comparable methods on how erodibility varies between the least disturbed mined landscapes and undisturbed ones. We prefer this over the alternative of directly comparing K values mapped from decades of post-mining gully erosion against Gallen (2018)'s natural K estimate that integrates over geologic time because of the dramatic mismatches between the two methods in spatial and temporal scale.

We measured the average depths, slopes, and drainage areas of 176 gullies from our five MTR-mined watersheds using 2018 lidar (1 m resolution; Fig. 3 shows an example). Each gully was assigned a minimum age based on the last year that the mine complex hosting the gully was mapped as actively mined in the Landsat-derived dataset of Pericak et al. (2018). Dividing gully depth by minimum age yields a maximum incision rate (Fig. 4). There is no clear relationship between gully incision rates and slope or drainage area, which suggests that variability in erosion rates might arise from mining-induced variations in land-surface erodibility. We use these gully incision rates along with their drainage area and slope to calculate a distribution of K within mined landscapes by rearranging the simple, detachment-limited form of the stream power incision model:

$$\frac{\partial z}{\partial t}_{\text{obs}} = -K_{\text{calc}} A^{0.5} S, \tag{4}$$

where $\frac{\partial z}{\partial t}_{\text{obs}}$ is the observed erosion rate (and is negative to indicate land-surface lowering), A is drainage area, and S is slope, to yield the inferred erodibility K_{calc}:

$$K_{\text{calc}} = \frac{-\frac{\partial z}{\partial t}_{\text{obs}}}{A^{0.5} S}. \tag{5}$$

We find an approximately two order of magnitude range in K_{calc} (Fig. 4). We take the median of the K_{calc} distribution to be the maximum extent to which erodibility exceeds the unmined value, thereby incorporating the bulk of our data while avoiding possible outliers (Fig. 4). Our calculated erodibilities, when scaled to the long-term background erodibility of Gallen (2018), therefore range from a minimum of $K_{\text{min}} = 1.30 \times 10^{-6}$ yr^{-1} on unmined landscapes to a maximum of $K_{\text{max}} = 3.4 \times 10^{-5}$ yr^{-1} on mined landscapes that have not yet experienced any vegetation recovery. We did not incorporate

MAP (i.e., use Eq. 2) in our gully incision analysis because our method yields only rough erodibility estimates and would not be improved by additional complexity; the difference in the dimensions of K between Eq. 2 and Eq. 5 is reconciled to first order by the fact that MAP is close to 1 m/yr in all of our study watersheds.

Because vegetation recovery trajectories depend so heavily on management decisions, and because there are no known relationships between vegetation recovery and land-surface erodibility, we explore the parameter space of vegetation recovery influences on erodibility by simulating three different vegetation recovery scenarios (Fig. 5). In each scenario, the erodibility immediately post-mining is the maximum value we inferred from our gully mapping ($K_{\max}$). K in each scenario then declines exponentially over 200 years—a rough timescale for full post-disturbance regeneration of Appalachian hardwood forests—towards a value $K^*_{\min}$, a minimum value imposed by the effectiveness of forest recovery. Our three-scenario analysis comprises a no-recovery case in which $K^*_{\min} = K_{\max}$, a full recovery case in which $K^*_{\min} = K_{\min}$, meaning that K declines from $K_{\max}$ to $K_{\min}$ over 200 years, and a 50% recovery case in which $K^*_{\min} = 0.5K_{\max}$, such that K declines from $K_{\max}$ to $0.5K_{\max}$ over 200 years. Figure 5 shows all three recovery scenarios, which are defined quantitatively by:

$$K^*_{\min} = K_{\max} - [(K_{\max} - K_{\min})P_r] \tag{6}$$

where P_r is the proportion of recovery (i.e., K returns $P_r \times 100\%$ of the way to its pre-mining value). We assume that K recovery trajectories over time follow a sublinear power law:

$$K = K_{\max} - [\frac{(K_{\max} - K^*_{\min})}{200^{0.25}}]t^{0.25}. \tag{7}$$

Here 200 is the 200 years roughly required for an Appalachian hardwood forest to develop from scratch, t is time since reclamation, and 0.25 is the exponent on the recovery curve we approximate from remote sensing vegetation recovery data (Ross et al., 2021; Thomas et al., 2022).

Once the 200 year recovery period is over, the K of mined portions of the landscape is held constant at $K^*_{\min}$. Physically, this means that there is some ceiling on the extent to which erodibility can recover that is reached after 200 years. K is only affected by mining on areas that Landsat imagery shows have been mined (Pericak et al., 2018); elsewhere on the landscape we

assume that $K = K_{\min}$ for all time because there was never any disturbance. This neglects other human disturbances to the landscape like logging, but allows us to specifically target the influence of MTR mining.

There is uncertainty inherent to Pericak et al. (2018)'s Landsat-based analysis of mined areas that we use to assign mined versus unmined K values. We therefore use a moving window to smooth K values across the landscape to account for 1) our lack of certainty about the exact boundary between mined and unmined areas given that their analysis has 30 m resolution while our DEMs have 10 m pixel size, and 2) potential spillover effects of mining onto areas mapped as unmined, like for example the development of service roads. We use a smoothing window of nine DEM cells, or 90×90 m, because Pericak et al. (2018) eliminated all mined areas $< 9,000$ m^2 from their analysis on the basis of uncertainty and using a nine-cell window means that we are smoothing K over an area as close to that threshold area as possible.

3.4.2. Sediment settling velocity

In our erosion–deposition model, the ratio of sediment erodibility K to effective settling velocity V governs how a landscape evolves. V is a quantity not equal to measured sediment settling velocity, but related to the net tendency towards deposition once effects of sediment concentration and upward-directed fluid forces are accounted for (Davy and Lague, 2009; Shobe et al., 2017). $\frac{K}{V} \gg 1$ shifts the system towards detachment-limited behavior and $\frac{K}{V} \ll 1$ shifts the system towards transport-limited behavior (Davy and Lague, 2009; Shobe et al., 2017). We treat V as an empirical constant that we infer from landscape characteristics. We use $V = 0.01$ m/yr because while field evidence indicates dominance of detachment-limited behavior in our study landscape (i.e., there is a preponderance of bedrock channels; Jaeger (2015)), there are thin mantles of alluvium in most stream valleys such that we cannot assume no contribution of transport-limited behavior. Because we calculated K values from detachment-limited stream power theory alone, by necessity implicitly assuming that settling velocity is negligible, we need now to modify our observed K values to account for the component of gully slope induced by settling with our assumed value of $V = 0.01$ m/yr. Equating the steady-state form of the detachment-limited stream power model with the steady-state form of the erosion–deposition model (Shobe et al., 2017) allows us to transform all observed K values (K_{obs}) to values for use in our simulations K_{sim} that account for the contribution of sediment deposition:

$$\frac{U}{K_{\text{obs}}A^m} = \frac{UV}{K_{\text{sim}}A^m P} + \frac{U}{K_{\text{sim}}A^m}, \tag{8}$$

which simplifies to:

$$K_{\text{sim}} = K_{\text{obs}}(\frac{V}{r} + 1). \tag{9}$$

These conversions allow us to acknowledge the mixed transport- and detachment-limited behavior of gullies and streams in our study area without adding undue model complexity. Whether our particular assumption of the value of V is correct or not, this approach allows model parameters to be constrained without assuming a purely detachment-limited system.

3.4.3. Precipitation and the influence of climate change

We set P for each catchment to be the catchment-averaged MAP. As a consequence of climate change, historical (or current) precipitation data is not a reasonable proxy for future precipitation. Previous post-mining studies have used spatial climate change analogues (Hancock et al., 2017b). However, recent work suggests that we are entering a regime where future climate in many locations globally does not have a spatial climate analog because of the magnitude of expected change (Dahinden et al., 2017). We therefore use climate projections derived from general circulation models (the NASA BioClim dataset; Pearson et al., 2014) to represent the future trends within each watershed. We take the average of BioClim's MAP product, a warming scenario that assumes CO_2 stabilization at 450 ppm, over each of our study watersheds for 2010–2100. After the first 90 years of simulation time we hold MAP constant at its 2100 value (e.g., Barnhart et al., 2020b), reasoning that changes beyond that timeline are unpredictable because they rest on human choices made over the rest of this century.

3.5. Initial and boundary conditions

All simulations begin from either the pre-mining or post-mining DEMs of Ross et al. (2016). The pre-mining DEM is derived from historical 10m USGS contour lines pre-dating 1970. The post-mining DEM is derived from ground-return lidar data flown in 2010 and resampled to the same cell size (10 m) as the pre-mining DEM (Ross et al., 2016). There is some inherent variability due to the vastly different data collection methods; it is negligible compared to the enormous topographic changes caused by MTR.

Each study watershed has no-flux boundary conditions imposed along the boundary of the drainage with the exception of the outlet node, which uses a Dirichlet boundary condition in which node elevation lowers at a regionally representative rock uplift/baselevel lowering rate of 27.5 m/Ma. All models run for 10 kyr in one-year timesteps during the recovery period and two-year timesteps for the remaining time.

4. Results

4.1. Sediment fluxes from mined and unmined watersheds

Our experiments allow us to isolate the influence of topography by comparing erosion between mined and unmined DEMs without incorporating any change in vegetation/erodibility, and then to assess the influence of erodibility by comparing among our different forest recovery scenarios.

When vegetation-controlled erodibility is held equal between mined and unmined landscapes, the total sediment flux from all five watersheds is universally lower in the mined case than the unmined case (Fig. 7). The total sediment exported over 10 kyr decreased by 8–26% among our five watersheds between model runs using the unmined DEM and the mined DEM. The two catchments in which sediment export changes least in percentage terms between the simulations using pre- and post-mining topography are Laurel Creek (11%) and Spruce Fork (8%), which are the two largest catchments and the two catchments in which mining covers the lowest proportion of the watershed (22% and 20%, respectively). Similarly, the two catchments that experienced the greatest proportional change in sediment flux between model runs using the pre- versus post-MTR topography, Mud River (26%) and White Oak (23%), are the smallest catchments and have the highest proportions of their area mined (38% and 31%, respectively).

Acknowledging the fact that mined portions of the landscape are likely to be initially more erodible—due to their lack of mature vegetation—than unmined portions of the landscape complicates the relationship between sediment export from mined catchments and sediment export from their unmined counterparts (Fig. 7). In the most optimistic recovery scenario, in which erodibility returns to its unmined value after 200 years, sediment export is 5-7% greater than the mined control case with no erodibility change but 4-21% less than the unmined case. The two additional revegetation scenarios, in which erodibility recovers 50% of the way towards its unmined value or does not recover at all, show much greater sediment export from the

mined catchments. The progressive increase in sediment export across the 100%, 50%, and 0% recovery cases is slightly less than linear. In the worst case (0% recovery) scenario, in which erodibility never declines from its high post-mining value, sediment export is 365%–888% higher than the mined case with no erodibility change and 326%–627% higher than the unmined case.

4.2. Temporal patterns in catchment-averaged erosion

Tracking cumulative sediment export from the study watersheds over the 200 year vegetation recovery timescale (Fig. 8, left column) and the remainder of the 10 kyr simulation (Fig. 8, right column) illustrates temporal erosion dynamics. All five watersheds exhibit similar patterns.

The unmined case and the mined case with no erodibility change show the same erosion trajectory over time, with only slightly differing volumes of erosion at any given time due to the presence/absence of mining-altered topography. The most salient differences between the cases in which erodibility is perturbed by mining (colored solid lines in Fig. 8) and those in which it is not (dashed lines in Fig. 8) occur in the first 200 years of the simulations, during the period of forest recovery. At the end of the 200 year recovery period, the worst-case (0%) vegetation recovery scenario produces 317–742% greater sediment export than the mined case with no erodibility perturbation, and 286–535% greater export than the unmined case. The best-case (100%) recovery scenario produces 71–156% greater sediment export than the mined case with no erodibility perturbation, and 58–93% greater export than the unmined case.

Vegetation recovery, or lack thereof, over the first 200 years governs the 10 kyr trajectory of erosion and sediment export (Fig. 8). The best-case (100%) recovery scenario approaches the mined case with no erodibility perturbation, with differences in total sediment export between the two cases declining from 71–156% after 200 years to 5-7% after 10 kyr. This scenario exhibits 4–21% less sediment export after 10 kyr than the unmined case despite having 58–93% greater export after 200 years. When there is no forest recovery, mining-induced increases in sediment export continue to grow over the full 10 kyr period. The difference between the worst-case (0%) recovery scenario and the mined and unmined control cases increases from 317–742% to 365–888% and 286–535% to 326–627%, respectively over the 9,800 years after the potential forest recovery period ends. Across all five watersheds, the mined control case, the unmined control case, and the 100% recovery case experience

sediment fluxes that decline over time from 200–10,000 yrs (Fig. 9). The 0% and 50% recovery cases, however, experience increases in sediment flux over the same time period.

4.3. Distributions of erosion rates

We assess the variability of erosion in space by plotting histograms of erosion rates for each catchment and model scenario (Fig. 10). Erosion rates are averages over the 10 kyr of model time; positive rates reflect net lowering of the landscape and negative rates reflect net deposition.

In all five watersheds, the erosion rate distribution is right-skewed to some extent, such that greater proportions of higher erosion rates than higher deposition rates are observed. In the unmined case and the mined case with no erodibility change, time-averaged erosion rates do not exceed 0.6 mm/yr anywhere in the study watersheds. The distribution is broader—that is, maximum erosion and deposition rates are greater—in the mined case with no erodibility change than in the unmined case. The distribution of erosion rates becomes progressively more skewed towards higher erosion rates as the extent to which the erodibility of mined areas recovers to its pre-mining state declines. The 100% recovery case exhibits an effectively identical distribution of 10 kyr average erosion and deposition rates to the mined case with no erodibility change. In the 0% recovery case, small proportions of the study catchments can experience erosion rates up to 3.5 mm/yr, approximately a six-fold increase from the mined case with no erodibility change. Maximum deposition rates decline approximately 20% from the mined case with no erodibility change to the 0% recovery case.

4.4. Spatial patterns in erosion rates

Erosion over the 10 kyr model runs is highly variable in space (Figs. 11 and 12 show the 50% recovery case in the White Oak watershed, but results hold across all five watersheds we investigated). While the magnitudes of erosion change based on the recovery scenario selected, the spatial patterns in erosion do not. In the unmined DEM (Fig. 11A) and the unmined portions of the mined catchment (Fig. 11B; left side of the DEM), erosion is fairly minimal (maximum of 6.4 m over 10 kyr; $<$1 m in most areas), except in locations where DEM artefacts (for example the DEM mosaicing and contour digitization artefacts visible in Fig. 12A) or non-MTR human alterations to the landscape (e.g., dams, roads) have driven minor erosion hotspots.

Erosion rates across most of the mined portion of the landscape are low, with the flattened ridgetop/filled valley topography experiencing <1 m of erosion on its flat surfaces (Figs. 11B and 12). Predicted erosion is greatest along the margins of the MTR-mined area, with magnitudes of erosion reaching up to 75.8 m over the 10 kyr period. The locations of the most rapid predicted erosion are steep valley fill faces, the scarps defining the edges of the mined areas (and scarps left by reclamation practices within mined areas), and the steep hillslopes just downslope of mined flats (Fig. 12). Predicted deposition reaches a maximum of 7.4 m over 10 kyr, and is concentrated primarily at the base of steep scarps and in low-order valleys, with more minor amounts in human-made impoundment structures on the mined surface (Fig. 12).

Combining information from the pre-mining DEM, the post-mining DEM, and the DEM after 10 kyr of simulated erosion across the three erodibility scenarios we tested allows us to assess the erosion trajectory of landforms unique to post-MTR region: valley fill faces (Fig. 13A and C), hillslopes adjacent to, but not within, the mined area (Fig. 13B), and a hillslope reshaped by mining (Fig. 13D). Each landform experiences progressively more erosion as the simulated recovery of post-mining erodibility towards its pre-mining state is reduced.

The valley fill faces (Fig. 13A and C) experience the anthropogenic addition of tens of meters of topography through the MTR mining process as headwater river valleys are transformed into waste rock deposits, followed by the most erosion of any post-MTR landform. We observe severe gullying in the two fills in Fig. 13A and C, with incision depths up to approximately 50 m below the post-mining land surface. The peripheral, but unmined, hillslope (Fig. 13B) experiences approximately 15 m of erosion by gullying. The altered hillslope (Fig. 13D), which experienced significant (up to 25 m) lowering of the topography over just a 40-year period through mining and reclamation, experiences diffusive relaxation of the steep scarp resulting in approximately five meters of surface lowering at the head of the scarp.

5. Discussion

5.1. Topographic and vegetation controls on post-MTR erosion

Our analysis isolates the relative influences of MTR-induced topographic change and vegetation disturbance under the assumption that vegetation influences land-surface erodibility. It also brackets the realm of possibility for

post-mining erosion, ranging from permanently and dramatically increased erodibility to full recovery of erodibility to its pre-mining state.

When quantifying the influence of topography alone, we find that mined watersheds produce less total sediment over 10 kyr than their unmined counterparts (Fig. 7). This occurs because the flattening of large portions of the landscape, due to both ridge lowering and valley filling, produces large regions with low slope and relatively low drainage area (Maxwell and Strager, 2013; Ross et al., 2016; Jaeger and Ross, 2021; Shobe et al., in review). The significant proportion of the study watersheds (20–38%) made up of this novel geomorphic unit means that the erosion-inhibiting effects of flattening outweigh the rapid erosion that occurs around the periphery of mined regions where flattened areas give way to steep natural or constructed hillslopes (Figs. 11 and 12; Reed and Kite (2020)) when no mining-induced erodibility changes are considered.

The assumption that MTR does not change land-surface erodibility, however, is likely not valid (Reed and Kite, 2020; Jaeger and Ross, 2021; Shobe et al., in review). When we relax this assumption and instead assume that erodibility increases immediately after mining and then declines over time as vegetation recovers (Fig. 5), we find that mined watersheds in which erodibility does not recover fully to its pre-mining value export more sediment over the next 10 kyr (Fig. 7) and experience higher peak erosion rates (Fig. 10) than their unmined counterparts. Given the maximum and minimum erodibility values we infer from our analysis of gullies on mined landscapes (Figs. 3 and 4), we find that even recovery of mined landscape erodibility 50% of the way to its pre-mining state allows efficient enough erosion that sediment export from mined watersheds far outpaces their unmined counterparts (Fig. 7). Intriguingly, 100% erodibility recovery results in less total sediment export from mined than unmined watersheds, indicating that under these conditions the brief increase in erodibility caused by mining is insufficient to overcome the erosion-reducing effect of slope reduction across the watershed. There exist no data on the relationship between post-MTR revegetation and erodibility, or on the extent to which the erodibility once vegetation has recovered might be altered by mining-induced material property changes, so we cannot assess the likelihood that mined watersheds in our study region reach this 50% recovered state or any other. Because we have been conservative in defining maximum erodibility as the median derived from our gully mapping, it is probable that forest recovery would need to be both very efficient and very complete to prevent mined watersheds from exporting more sediment

than unmined ones.

Erosion rates are highest in our mined study watersheds (Fig. 8) for the first few decades after mining because of complementary ecological and geomorphic factors. Forest recovery on reclaimed mines seems to approximate a sublinear power-law function whereby vegetation recovers quickly at first and then more slowly as it nears (but never reaches) its natural state (e.g., Ross et al., 2021; Thomas et al., 2022). Because we have assumed that erodibility recovers in tandem with vegetation, most erosion and sediment export in our study watersheds occurs in the first century while erodibility is much greater than both its pre-mining value and the value it will ultimately reach after vegetation recovers to its maximum possible extent (i.e., 50% or 100% of the way to its pre-mining state). The occurrence of peak erosion rates immediately after mining is also driven by geomorphology. Slopes on human-constructed topographic features are steepest immediately post-mining, and decline over time as erosion proceeds.

We can think of post-MTR regions as a set of steep-edged plateaus being incised by a resurgent drainage network. In these landscapes, the relative influence of land-surface erodibility and initial topography govern whether catchment-averaged erosion rates increase or decline over the first 10 kyr of landscape evolution. We observe both cases in which high erodibility allows rapid expansion of the drainage network, steepening of previously flattened slopes, and resulting increases in catchment-averaged erosion rates over time (the 0% and 50% recovery scenarios in Fig. 9), as well as cases in which low erodibility precludes the expansion of erosion hotspots over our simulation timescale and causes a decline in catchment-averaged erosion rates over time (the 100% recovery and control scenarios in Fig. 9). The existence of this critical restoration threshold, consistent across all five watersheds, suggests that efficiently returning mined land erodibility to its pre-mining condition may not only reduce the magnitude of sediment export at any given time, but also set mined watersheds on a desirable path of declining sediment flux over time. Failing to return mined lands to near their pre-mining erodibility may, in addition to causing greater sediment export immediately post-reclamation, lock in millennia of steadily increasing sediment fluxes.

Post-mining topography is a fixed initial condition that imposes a fairly minor reduction in erosion due to topography alone (Fig. 7), so the extent to which a post-MTR landscape erodes depends primarily on the extent to which its erodibility increases above, and fails to decline to, the pre-mining condition. This control can be conceptualized as the erodibility integrated

over time, a quantity that can be increased by greater mining-driven increases in initial post-mining erodibility, slower recovery of erodibility towards its post-mining state, and/or a greater erodibility even after recovery is complete due to ineffective revegetation or permanent mining-induced material property changes (Fig. 5). Our findings are consistent with empirical modeling suggesting that the vegetated state of the post-MTR landscape governs short-term erosion (Sears et al., 2020), and further points to short-term vegetation recovery as remaining a key control on sediment export over millennia.

Vegetation is not the only control on erodibility in post-MTR landscapes. Our modeling effort neglects other changes in material properties caused by MTR mining, such as the construction of valley fills and minesoils (Shobe et al., in review), that likely set the extent to which post-mining landscapes can recover towards their pre-mining erodibility.

5.2. Processes driving hotspots of post-mining landscape change

The margins of MTR landscapes, where mined areas meet unmined areas, are the primary hotspots of erosion in our experiments. Erosion hotspots can arise due to gully erosion in areas of drainage network expansion or due to efficient hillslope sediment transport along steep scarps.

Valley fill faces, the stairstep-like topographic elements that delineate the edges of waste rock deposits filling former stream valleys, erode faster than anywhere else on the landscape (Figs. 11– 13). This occurs because valley fills are the portions of the post-MTR landscape that are most out of slope–area equilibrium: their drainage area tends to remain high because they occupy the sites of former low-order streams, but the average slope of valley fill faces can reach nearly 0.5 m/m, several times to an order of magnitude greater than the slopes of headwater streams in the region. This combination of high slope and drainage area drives rapid erosion in our simulations. Though simple landscape evolution models do not make distinctions between ephemeral gullies and stable perennial stream channels, we interpret the incision of valley fills to be a gullying process in which the channel network is effectively re-establishing itself by incising steep, artificial hillslopes placed in locations of high drainage area.

Outside of valley fills, the hillslopes below mined mountaintops also experience significant erosion in our models (Figs. 11– 13). Gullies incising mine-adjacent sideslopes that do not themselves fall within the mined area are deepest at the top of the slope near the mined area, and become shallower as they grade towards the valley floor. We observe this result because

of our choice to smooth the erodibility across the landscape using a moving window: erodibility smoothly transitions from its mined value to its unmined value across a distance of 90 m, or nine grid cells. Enhanced erodibility at the top of mine-adjacent hillslopes therefore allows efficient gullying, while lower erodibility at the bottom of the same hillslopes causes reduced gully incision.

Observations of gully incision into valley fills and sideslopes along the periphery of mined areas in our numerical simulations agree with field observations from MTR landscapes (Reed and Kite, 2020). Reed and Kite (2020) found that post-MTR landscapes exhibited high gully densities along the edges of mined areas—a maximum of five gullies per km^2 of area mined—and that up to 25% of the gullies along the margin of a given mine occurred on valley fills. Though they did not pinpoint a cause for each gully, Reed and Kite (2020) suggested possible causes of gully formation. On valley fill faces, gullying likely occurs due to the marked geomorphic disequilibrium of the landform combined with its lack of vegetation and potentially less erosion-resistant material properties. On undisturbed sideslopes below mined areas, there are no significant vegetation or material property changes, and Reed and Kite (2020) suggested that gullying in these areas is driven by pulses of stormwater runoff from reclaimed mines just upslope. They noted that some sideslope gullies occur just below retention cells, human-made structures designed to retard runoff from mined landscapes, suggesting a hydrologic control on gully incision.

In light of field observations, we suggest that our model reasonably captures the mechanisms driving gullying on valley fills but not on mine-adjacent sideslopes. Valley fills are mapped as mined areas in our forcing data, so experience greater erodibility than nearby unmined areas. Increased erodibility on valley fills, combined with their improbable position in slope–area space, drives expansion of the drainage network by gullying. Our model does not capture the mechanisms driving sideslope gullying except in a heuristic way. We observe sideslope gullying because of the way we smooth transitions in erodibility between mined and unmined landscapes, while the real driver is thought to be pulses of stormwater runoff (Reed and Kite, 2020), a forcing not simulated in our models that simply scale water discharge with drainage area and assume steady, uniform flow. To capture these dynamics, our model would need at minimum spatially variable runoff generation.

While the greatest predicted erosion depths occur on valley fills due to their steep slopes, high drainage areas, and high erodibilities, we also observe

significant erosion and deposition along human-made scarps both within and along the periphery of mined areas (Figs. 11— 13). Scarp erosion is the only natural means of redistributing mass on mined summit flats, where drainage networks cannot re-establish themselves except by many millennia of bedrock-erosion-driven lateral retreat of adjacent hillslopes. Scarp erosion is responsible for the highest quantities of sediment deposition observed in our study as sediment accumulates along mined flats at the base of scarps. The extent to which our predictions of scarp erosion and deposition are reasonable depends primarily on the material properties of engineered scarps. In cases where they are constructed of mine spoil, our predicted along-scarp erosion and deposition depths may be close to minimum values given that we did not allow vegetation, or lack thereof, to influence the efficiency of hillslope processes. When scarps are cut into bedrock, our estimates are likely close to maximum possible values. Mined scarps also often tend to fail in mass-wasting events (Bell et al., 1989), suggesting that the linear diffusion approximation for hillslope processes describes the long-term average result of scarp evolution rather than event-scale erosion dynamics.

While our assumption of a mostly detachment-limited landscape ($V = 0.01$ m/yr) ensures that maximum deposition rates are substantially lower than maximum erosion rates (Fig. 10) and that most eroded sediment is exported from the watersheds, rapid erosion of the margins of MTR-mined areas results in net sediment accumulation in colluvial hollows and headwater river valleys (Fig. 12). The combined effects of efficient gully erosion along mine margins and hillslope sediment transport down steep hillslopes and valley fill faces results in sediment supply to headwater valleys that, on average, exceeds fluvial transport capacity. One implication of this focused deposition is the potential for increased debris flow activity. MTR mining may drive erosion patterns that efficiently load steep, low-order channels with sediment that could then fail during subsequent storm events. Though MTR mountaintops themselves are, due to being nearly perfectly flat, devoid of any debris flow activity (Jaeger and Ross, 2021), MTR may have the effect of pushing the debris flow process domain into areas of slope–area space that were previously dominated by fluvial processes. There is currently no data on the relationship between MTR mining and spatiotemporal patterns of debris flows, but the potential for MTR to shift debris flow locations and dynamics is worth considering given the prevalence of debris flows as agents of Appalachian landscape evolution (e.g., Eaton et al., 2003) and geomorphic hazards (e.g., Wieczorek and Morgan, 2008).

Substantial sediment deposition in headwater streams, if model predictions are realized, would contribute to MTR's well-studied negative impacts on aquatic ecosystems (e.g., Bernhardt and Palmer, 2011). High sedimentation rates are destructive to the endangered endemic amphibian species that make central Appalachia a critical biodiversity hotspot (Wiley, 2001). Field evidence, however, is mixed on the extent to which MTR mining drives sedimentation in headwater streams. Rates of delivery of fine sediment to channels do seem to be greater in mined areas relative to unmined areas (Jaeger, 2015; Wiley, 2001), but some observations show increased bedrock exposure in streams that drain mined areas relative to those that do not (Jaeger, 2015). It is possible that mining-induced changes to land-surface hydrology, or explicit treatment of multiple grain sizes, would need to be added to our model to better capture headwater sediment dynamics, but our simulations indicate that there is some risk of ecologically destructive sedimentation over the long term in headwater streams that drain heavily mined areas. Our results do not indicate that sedimentation persists in second- and third-order streams; transport capacity outcompetes sediment supply in those channels as unmined areas make up a greater proportion of upslope area. We emphasize, however, that modeled sedimentation rates and volumes depend heavily on the choice of the effective settling velocity V. If transport-limited process dynamics are found to matter in these streams to a greater extent than we have modeled (i.e., if $V \gg 0.01$ m/yr), we should expect more sedimentation than our current set of results predicts.

5.3. Implications for management

By elucidating the spatiotemporal dynamics of post-MTR landscape change, our results suggest that improved revegetation trajectories can reduce peak sediment fluxes from newly reclaimed mines, but that the geomorphic character of reclaimed MTR mines means that above-background erosion rates are all but inevitable over millennial timescales.

During the first few decades after mining when managers have the most control, the revegetation trajectory of reclaimed MTR mines is critical. Peak sediment export from mined watersheds occurs in the first few years following reclamation. Reductions in post-mining erodibility can smooth out initial sediment pulses over longer time periods, potentially mitigating harm to aquatic ecosystems. This involves reducing the maximum (presumably immediately post-mining) erodibility, the recovery timescale, and the erodibility the landscape reaches after full recovery of vegetation to the extent

possible given local growing conditions. Reclamation approaches that specifically target the restoration of forests (e.g., Zipper et al., 2011) have the potential to reduce post-mining erosion over annual to decadal timescales, but that potential remains unstudied.

Over millennial timescales, MTR landforms will always erode back towards their prior, self-organized state. Even our scenarios in which erodibility is not perturbed by mining—an unlikely possibility—show that valley fill faces are erosion hotspots, an outcome that agrees with field observations (Reed and Kite, 2020). This suggests that as long as mine reclamation involves building valley fill landforms that have high slope and high drainage area, flowing water will always leverage the resulting geomorphic disequilibrium to re-establish a drainage network, driving erosion of the valley fill surface that will outpace that of adjacent natural landforms. Even establishing engineered, armored channels along the margins of valley fills has proven ineffective at stopping gullying in both modeling (Sears et al., 2020) and field (Reed and Kite, 2020) analyses. Our work speaks to the importance of practices like Geomorphic Landform Design (e.g., Hancock et al., 2003; Lowry et al., 2013; DePriest et al., 2015; Hancock et al., 2020a) the practice of building landforms that have slope–area distributions as similar as possible to the pre-mining landscape. In MTR regions this effectively means reducing the mean slope of valley fill faces (DePriest et al., 2015).

5.4. Limitations and opportunities

This study contains a number of simplifications and assumptions that future work on post-MTR landscape evolution might be able to relax.

Post-MTR landscapes have complex spatial distributions of material properties (Shobe et al., in review). In our model we assume that the entire landscape is underlain by a single material, as opposed to distinguishing between sediment and bedrock (Shobe et al., 2017). We also assume that the only control on the erodibility of mined areas is the extent of vegetation recovery, such that there is no change in the eroibility driven purely by changes to surface material properties. But differences between mine soils at the reclaimed surface, the crushed waste rock of valley fills, and the natural soil column of adjacent unmined areas likely influence rates of geomorphic change by both fluvial and hillslope processes.

We neglect processes of hillslope failure in our models. However, field observations show that valley fills can experience landslides (Reed and Kite, 2020), and debris flows are a common agent of geomorphic change in unmined

Appalachian landscapes (Wieczorek and Morgan, 2008). Though post-MTR landscapes may be on average less susceptible to hillslope failures than their unmined counterparts due to the loss of much of the colluvial process domain (Jaeger and Ross, 2021), a more complete model of post-mining landscape change would include these processes and their interactions with the fluvial system (e.g., Campforts et al., 2022).

The most significant simplifications in our modeling effort relate to land-surface hydrology. We assumed spatially uniform generation of overland flow by asserting that fluvial erosion is proportional to upstream area. However, most field evidence points toward post-MTR landscapes having three unique hydrologic domains: cut areas that efficiently generate overland flow because thin soils overlie less permeable bedrock; filled areas that efficiently absorb large quantities of water and act as subsurface reservoirs; and unmined areas that exhibit intermediate behavior (Nippgen et al., 2017; Shobe et al., in review). We also assume steady, uniform overland flow through the use of a stream-power-type model. Reed and Kite (2020) suggested that much of the gully erosion occurring on the periphery on mined areas occurs due to overtopping of, or intentional discharge from, stormwater retention cells. If the timing and location of most post-mining erosion is driven by the spatiotemporal distribution of pulses of peak flow, more complex treatments of hydrology and hydraulics that include 1) spatial variability in runoff generation, 2) unsteady, nonuniform flow, and 3) erosion thresholds, will produce more useful predictions. It also might be worth exploring the interplay between vegetation recovery and surface hydrology, as our models assume that there are no feedbacks between these processes. Finally, D8 flow routing is probably not appropriate for post-MTR summit flats, where extremely low slopes are likely to cause diverging flow that requires a different approach (e.g., Tarboton, 1997).

Control simulations run from pre-MTR DEMs should not be construed as representing the dynamics of completely natural landscapes. Though the pre-MTR DEMs do pre-date widespread MTR mining, they incorporate two centuries of human disturbances to the Appalachian landscape from logging to underground mining to bench-and-highwall contour mining, all of which influence surface processes. While the pre- and post-mining comparison in our study allows us to elucidate how MTR specifically affects landscape evolution trajectories, and simulations run from pre-MTR DEMs provide the best approximation we have of how an undisturbed landscape might evolve, there are no truly undisturbed Appalachian landscapes.

6. Conclusions

We leveraged an experiment in large-scale human landscape modification to assess the influences of topography and vegetation on post-mining geomorphic change in MTR-mined drainage basins. We first compared the evolution of unmined versus mined topography under the assumption of no vegetation change. We then incorporated the effects of post-mining revegation by using erodibility values derived from gully mapping of mined landscapes to parameterize how the erodibility of mined areas changes as a function of time since mining. We found that:

1. When considering topographic effects alone, MTR reduces total sediment export because the creation of large summit flats outweighs the effects of erosion hotspots on valley fill faces.
2. When post-mining erodibility recovers less than 100% of the way to its pre-mining state, sediment export from post-mining watersheds exceeds that of unmined watersheds.
3. Erosion is most rapid during the first few decades post-mining before substantial vegetation recovery can occur, but the extent of vegetation recovery also governs the 10 kyr—long beyond the recovery timescale—trajectory of sediment fluxes from mined lands. A threshold exists between 100% and 50% recovery that sets whether sediment fluxes increase or decrease over time after recovery has ceased.
4. Sediment export from mined lands is set by the integrated erodibility over time, a function of how dramatic the disturbance in erodibility is, how long it lasts, and the level to which it recovers.
5. Erosion is concentrated on valley fill faces where artificial landforms create slope–area disequilibrium, and along steep mine scarps.
6. Deposition is greatest at the base of scarps and in low-order stream valleys, where it has the potential to harm endangered aquatic species.

Our results quantify the response of Appalachian landscapes to MTR mining over millennial timescales. Potential paths towards improved reclamation outcomes emerge from our work. Over the short term, improving erosion control during the first few decades post-mining when vegetation recovery is in its early stages can reduce sediment fluxes and the potential for negative ecological effects like headwater stream sedimentation. Over the long term, ensuring that vegetation is restored as closely as possible to

its pre-mining state can set sediment export on a downward trajectory over time, and reducing the occurrence of dramatic slope–area disequilibrium can prevent the formation of erosion hotspots. If the renewable energy transition drives an increase in surface mining, drawing lessons from the past half-century of MTR mining will allow us to avoid repeating past mistakes, improve reclamation outcomes, and minimize disturbances to geomorphic and environmental systems.

Acknowledgements

This work was supported by the NASA Established Program to Stimulate Competitive Research, grant #80NSSC19M0054 (NASA West Virginia Space Grant Consortium). We acknowledge time on the West Virginia University Thorny Flat high-performance computing cluster, which is supported by the NSF under MRI award #1726534. We thank Leslie Hopkinson, Steve Kite, Rick Landenberger, and Miles Reed for helpful discussions.

Data availability

Data will be made publicly and permanently available in a DOI-stamped FigShare repository upon submission of the revised manuscript.

References

Barnes, R., 2017. Parallel non-divergent flow accumulation for trillion cell digital elevation models on desktops or clusters. Environmental Modelling & Software 92, 202–212.

Barnhart, K.R., Hutton, E.W., Tucker, G.E., Gasparini, N.M., Istanbulluoglu, E., Hobley, D.E., Lyons, N.J., Mouchene, M., Nudurupati, S.S., Adams, J.M., et al., 2020a. Landlab v2. 0: a software package for earth surface dynamics. Earth Surface Dynamics 8, 379–397.

Barnhart, K.R., Tucker, G.E., Doty, S.G., Glade, R.C., Shobe, C.M., Rossi, M.W., Hill, M.C., 2020b. Projections of landscape evolution on a 10,000 year timescale with assessment and partitioning of uncertainty sources. Journal of Geophysical Research: Earth Surface 125, e2020JF005795.

Bell, J.C., Daniels, W.L., Zipper, C.E., 1989. The practice of "approximate original contour" in the central appalachians. i. slope stability and erosion potential. Landscape and Urban Planning 18, 127–138.

Bernhardt, E.S., Palmer, M.A., 2011. The environmental costs of mountaintop mining valley fill operations for aquatic ecosystems of the central appalachians. Annals of the New york Academy of Sciences 1223, 39–57.

Campforts, B., Shobe, C.M., Overeem, I., Tucker, G.E., 2022. The art of landslides: How stochastic mass wasting shapes topography and influences landscape dynamics. Journal of Geophysical Research: Earth Surface 127, e2022JF006745.

Culling, W., 1963. Soil creep and the development of hillside slopes. The Journal of Geology 71, 127–161.

Dahinden, F., Fischer, E.M., Knutti, R., 2017. Future local climate unlike currently observed anywhere. Environmental Research Letters 12, 084004.

Davy, P., Lague, D., 2009. Fluvial erosion/transport equation of landscape evolution models revisited. Journal of Geophysical Research: Earth Surface 114.

DePriest, N.C., Hopkinson, L.C., Quaranta, J.D., Michael, P.R., Ziemkiewicz, P.F., 2015. Geomorphic landform design alternatives for an existing valley fill in central appalachia, usa: Quantifying the key issues. Ecological Engineering 81, 19–29.

van Doorn, J., Ly, A., Marsman, M., Wagenmakers, E.J., 2020. Bayesian rank-based hypothesis testing for the rank sum test, the signed rank test, and spearman's ρ. Journal of Applied Statistics 47, 2984–3006.

Eaton, L.S., Morgan, B.A., Kochel, R.C., Howard, A.D., 2003. Role of debris flows in long-term landscape denudation in the central appalachians of virginia. Geology 31, 339–342.

Evans, K., Willgoose, G., 2000. Post-mining landform evolution modelling: 2. effects of vegetation and surface ripping. Earth Surface Processes and Landforms: The Journal of the British Geomorphological Research Group 25, 803–823.

Feng, Y., Wang, J., Bai, Z., Reading, L., 2019. Effects of surface coal mining and land reclamation on soil properties: A review. Earth-Science Reviews 191, 12–25.

Gallen, S.F., 2018. Lithologic controls on landscape dynamics and aquatic species evolution in post-orogenic mountains. Earth and Planetary Science Letters 493, 150–160.

Greer, B.M., Burbey, T.J., Zipper, C.E., Hester, E.T., 2017. Electrical resistivity imaging of hydrologic flow through surface coal mine valley fills with comparison to other landforms. Hydrological Processes 31, 2244–2260.

Guebert, M.D., Gardner, T.W., 2001. Macropore flow on a reclaimed surface mine: infiltration and hillslope hydrology. Geomorphology 39, 151–169.

Hancock, G., Duque, J.M., Willgoose, G., 2020a. Mining rehabilitation–using geomorphology to engineer ecologically sustainable landscapes for highly disturbed lands. Ecological Engineering 155, 105836.

Hancock, G., Evans, K., Willgoose, G., Moliere, D., Saynor, M., Loch, R., 2000. Medium-term erosion simulation of an abandoned mine site using the siberia landscape evolution model. Soil Research 38, 249–264.

Hancock, G., Loch, R., Willgoose, G., 2003. The design of post-mining landscapes using geomorphic principles. Earth Surface Processes and Landforms: The Journal of the British Geomorphological Research Group 28, 1097–1110.

Hancock, G., Lowry, J., Coulthard, T., 2015. Catchment reconstruction—erosional stability at millennial time scales using landscape evolution models. Geomorphology 231, 15–27.

Hancock, G., Lowry, J., Coulthard, T., 2016. Long-term landscape trajectory—can we make predictions about landscape form and function for post-mining landforms? Geomorphology 266, 121–132.

Hancock, G., Saynor, M., Lowry, J., Erskine, W., 2020b. How to account for particle size effects in a landscape evolution model when there is a wide range of particle sizes. Environmental Modelling & Software 124, 104582.

Hancock, G., Verdon-Kidd, D., Lowry, J., 2017a. Sediment output from a post-mining catchment–centennial impacts using stochastically generated rainfall. Journal of Hydrology 544, 180–194.

Hancock, G., Verdon-Kidd, D., Lowry, J., 2017b. Soil erosion predictions from a landscape evolution model–an assessment of a post-mining landform using spatial climate change analogues. Science of the Total Environment 601, 109–121.

Hancock, G.R., Willgoose, G.R., 2021. Predicting gully erosion using landform evolution models: Insights from mining landforms. Earth Surface Processes and Landforms 46, 3271–3290.

Hooke, R.L., 1999. Spatial distribution of human geomorphic activity in the united states: comparison with rivers. Earth Surface Processes and Landforms: The Journal of the British Geomorphological Research Group 24, 687–692.

Hooke, R.L., 2000. On the history of humans as geomorphic agents. Geology 28, 843–846.

Howard, A.D., Kerby, G., 1983. Channel changes in badlands. Geological Society of America Bulletin 94, 739–752.

Jaeger, K., Ross, M., 2021. Identifying geomorphic process domains in the synthetic landscapes of west virginia, usa. Journal of Geophysical Research: Earth Surface 126, e2020JF005851.

Jaeger, K.L., 2015. Reach-scale geomorphic differences between headwater streams draining mountaintop mined and unmined catchments. Geomorphology 236, 25–33.

Kwang, J., Thaler, E., Larsen, I., 2023. The future of soils in the midwestern united states. Earth's Future 11, e2022EF003104.

Lowry, J., Coulthard, T., Hancock, G., 2013. Assessing the long-term geomorphic stability of a rehabilitated landform using the caesar-lisflood landscape evolution model, in: Mine closure 2013: Proceedings of the eighth international seminar on mine closure, Australian Centre for Geomechanics. pp. 611–624.

Lowry, J., Narayan, M., Hancock, G., Evans, K., 2019. Understanding post-mining landforms: Utilising pre-mine geomorphology to improve rehabilitation outcomes. Geomorphology 328, 93–107.

Maxwell, A.E., Strager, M.P., 2013. Assessing landform alterations induced by mountaintop mining. Natural Science 5, 229–237.

Miller, A.J., Zégre, N.P., 2014. Mountaintop removal mining and catchment hydrology. Water 6, 472–499.

Negley, T.L., Eshleman, K.N., 2006. Comparison of stormflow responses of surface-mined and forested watersheds in the appalachian mountains, usa. Hydrological Processes: An International Journal 20, 3467–3483.

Nippgen, F., Ross, M.R., Bernhardt, E.S., McGlynn, B.L., 2017. Creating a more perennial problem? mountaintop removal coal mining enhances and sustains saline baseflows of appalachian watersheds. Environmental science & technology 51, 8324–8334.

Pearson, R.G., Stanton, J.C., Shoemaker, K.T., Aiello-Lammens, M.E., Ersts, P.J., Horning, N., Fordham, D.A., Raxworthy, C.J., Ryu, H.Y., McNees, J., et al., 2014. Life history and spatial traits predict extinction risk due to climate change. Nature Climate Change 4, 217–221.

Pelletier, J.D., Brad Murray, A., Pierce, J.L., Bierman, P.R., Breshears, D.D., Crosby, B.T., Ellis, M., Foufoula-Georgiou, E., Heimsath, A.M., Houser, C., et al., 2015. Forecasting the response of earth's surface to future climatic and land use changes: A review of methods and research needs. Earth's Future 3, 220–251.

Pericak, A.A., Thomas, C.J., Kroodsma, D.A., Wasson, M.F., Ross, M.R., Clinton, N.E., Campagna, D.J., Franklin, Y., Bernhardt, E.S., Amos, J.F., 2018. Mapping the yearly extent of surface coal mining in central appalachia using landsat and google earth engine. PloS one 13, e0197758.

Phillips, J.D., 2004. Impacts of surface mine valley fills on headwater floods in eastern kentucky. Environmental Geology 45, 367–380.

Portenga, E.W., Bierman, P.R., Trodick, C.D., Greene, S.E., DeJong, B.D., Rood, D.H., Pavich, M.J., 2019. Erosion rates and sediment flux within the

potomac river basin quantified over millennial timescales using beryllium isotopes. GSA Bulletin 131, 1295–1311.

Reed, M., Kite, S., 2020. Peripheral gully and landslide erosion on an extreme anthropogenic landscape produced by mountaintop removal coal mining. Earth Surface Processes and Landforms 45, 2078–2090.

Richardson, P.W., Perron, J.T., Schurr, N.D., 2019. Influences of climate and life on hillslope sediment transport. Geology 47, 423–426.

Ross, M.R., McGlynn, B.L., Bernhardt, E.S., 2016. Deep impact: Effects of mountaintop mining on surface topography, bedrock structure, and downstream waters. Environmental science & technology 50, 2064–2074.

Ross, M.R., Nippgen, F., McGlynn, B.L., Thomas, C.J., Brooks, A.C., Shriver, R.K., Moore, E.M., Bernhardt, E.S., 2021. Mountaintop mining legacies constrain ecological, hydrological and biogeochemical recovery trajectories. Environmental Research Letters 16, 075004.

Sears, A., Hopkinson, L., Quaranta, J., 2020. Predicting erosion at valley fills with two reclamation techniques in mountainous terrain. International Journal of Mining, Reclamation and Environment 34, 223–237.

Shobe, C.M., 2022. How impervious are solar arrays? on the need for geomorphic assessment of energy transition technologies. Earth Surface Processes and Landforms 47, 3219–3223.

Shobe, C.M., Bower, S.J., Maxwell, A.E., Rachel, G.C., Samassi, N.M., in review. The uncertain future of mountaintop-removal-mined landscapes 1: How mining changes erosion processes and variables. Geomorphology .

Shobe, C.M., Tucker, G.E., Barnhart, K.R., 2017. The space 1.0 model: a landlab component for 2-d calculation of sediment transport, bedrock erosion, and landscape evolution. Geoscientific Model Development 10, 4577–4604.

Simon, A., Collison, A.J., 2002. Quantifying the mechanical and hydrologic effects of riparian vegetation on streambank stability. Earth surface processes and landforms 27, 527–546.

Skousen, J., Zipper, C.E., 2014. Post-mining policies and practices in the eastern usa coal region. International journal of coal science & technology 1, 135–151.

Skousen, J., Zipper, C.E., 2021. Coal mining and reclamation in appalachia, in: Appalachia's Coal-Mined Landscapes. Springer, pp. 55–83.

Sonter, L.J., Ali, S.H., Watson, J.E., 2018. Mining and biodiversity: key issues and research needs in conservation science. Proceedings of the Royal Society B 285, 20181926.

Sovacool, B.K., Ali, S.H., Bazilian, M., Radley, B., Nemery, B., Okatz, J., Mulvaney, D., 2020. Sustainable minerals and metals for a low-carbon future. Science 367, 30–33.

Tarboton, D.G., 1997. A new method for the determination of flow directions and upslope areas in grid digital elevation models. Water resources research 33, 309–319.

Thomas, C.J., Shriver, R.K., Nippgen, F., Hepler, M., Ross, M.R., 2022. Mines to forests? analyzing long-term recovery trends for surface coal mines in central appalachia. Restoration Ecology , e13827.

Tucker, G.E., 2009. Natural experiments in landscape evolution. Earth Surface Processes and Landforms 34, 1450–1460.

Tucker, G.E., Hancock, G.R., 2010. Modelling landscape evolution. Earth Surface Processes and Landforms 35, 28–50.

Vidal, O., Goffé, B., Arndt, N., 2013. Metals for a low-carbon society. Nature Geoscience 6, 894–896.

Wickham, J., Wood, P.B., Nicholson, M.C., Jenkins, W., Druckenbrod, D., Suter, G.W., Strager, M.P., Mazzarella, C., Galloway, W., Amos, J., 2013. The overlooked terrestrial impacts of mountaintop mining. BioScience 63, 335–348.

Wieczorek, G.F., Morgan, B.A., 2008. Debris-flow hazards within the Appalachian Mountains of the Eastern United States. US Department of the Interior, US Geological Survey.

Wiley, J.B., 2001. Reconnaissance of stream geomorphology, low streamflow, and stream temperature in the mountaintop coal-mining region, southern West Virginia, 1999-2000. volume 1. US Department of the Interior, US Geological Survey.

Wilkinson, B.H., 2005. Humans as geologic agents: A deep-time perspective. Geology 33, 161–164.

Willgoose, G., Riley, S., 1998. The long-term stability of engineered landforms of the ranger uranium mine, northern territory, australia: application of a catchment evolution model. Earth Surface Processes and Landforms: The Journal of the British Geomorphological Group 23, 237–259.

Zipper, C.E., Burger, J.A., Skousen, J.G., Angel, P.N., Barton, C.D., Davis, V., Franklin, J.A., 2011. Restoring forests and associated ecosystem services on appalachian coal surface mines. Environmental management 47, 751–765.

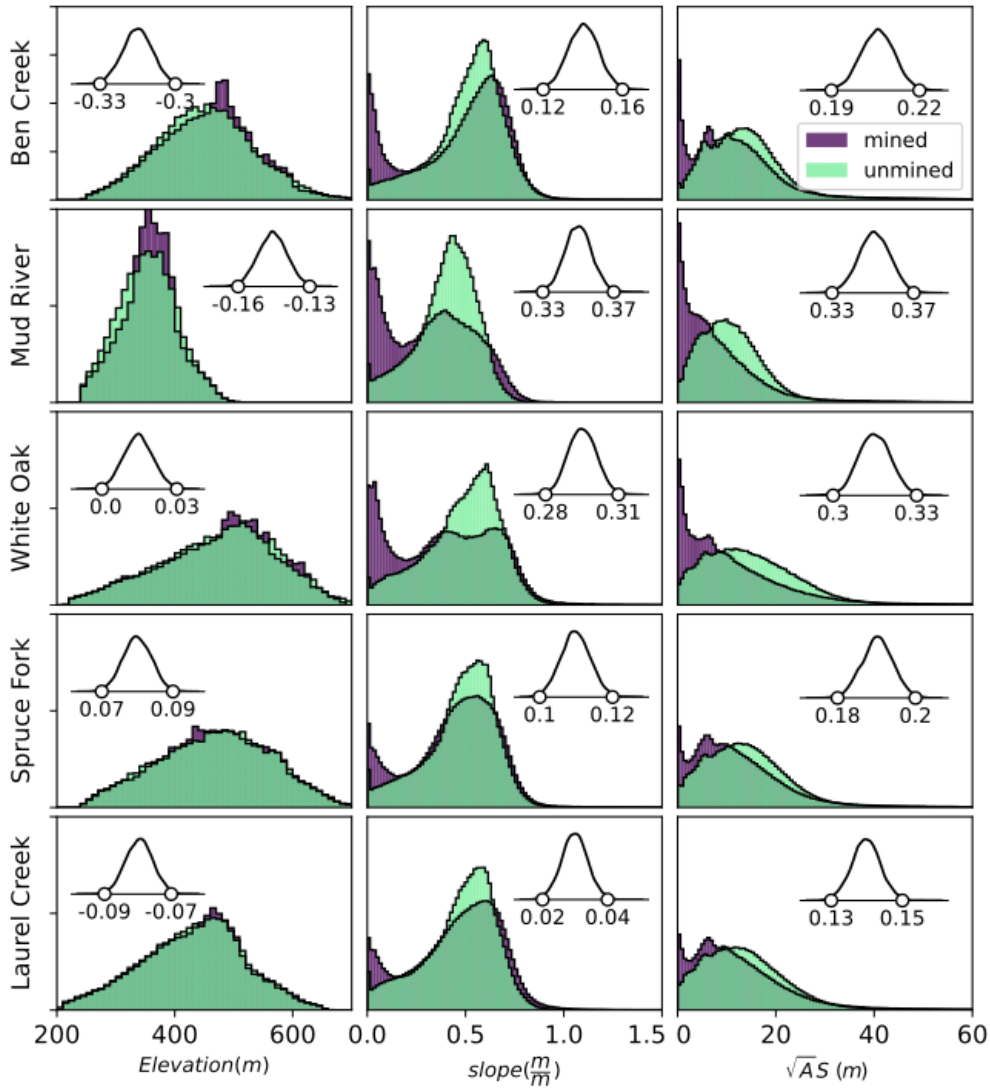

Figure 2: Differences in pre- and post-mining watershed topography. Histograms show the density of data as a count of pixels in pre-mined and post-mined catchments. The inset density curve in each panel is the distribution of the test statistic from Bayesian Wilcoxon signed rank tests (van Doorn et al., 2020) comparing the two distributions. Points and labels mark the edges of the 99% highest posterior density interval (HPDI) for the posterior distribution of the test statistic. We consider the distributions to be significantly different if the 99% HPDI does not include zero. $\sqrt{AS}$ is the slope–area product, a proxy for the efficacy of erosion by flowing water.

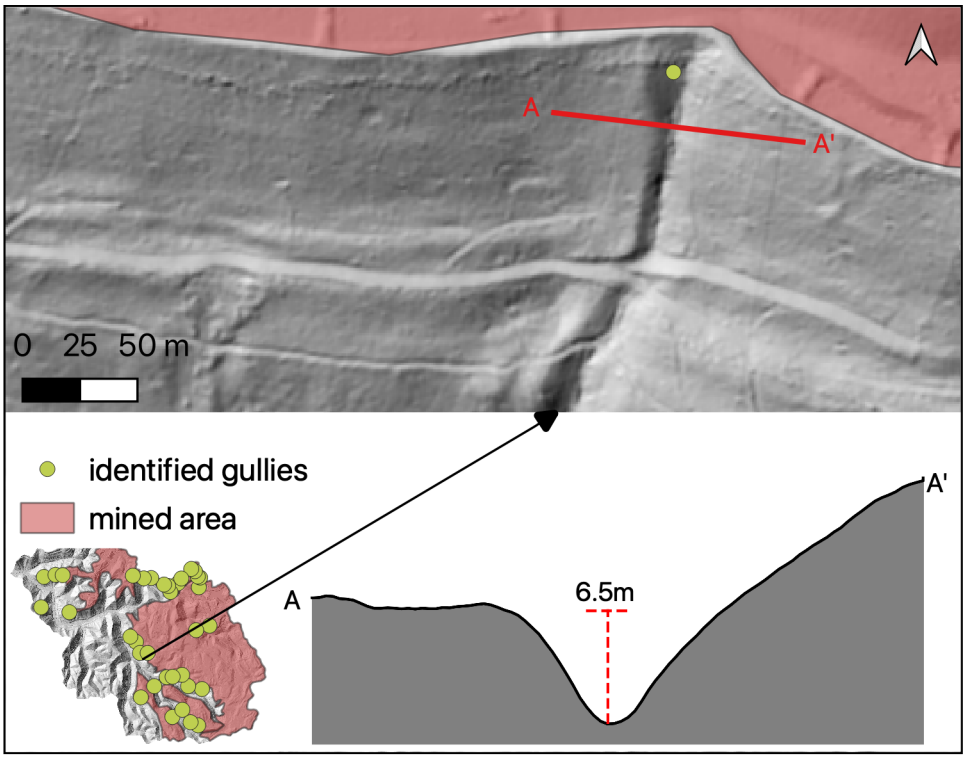

Figure 3: Lidar hillshade in the upper panel shows a gully identified on a peripheral hillslope in the White Oak watershed (approximate coordinates: 38.03°N, 81.51°W). This gully is representative of much of the fluvial incision occuring on mining-adjacent hillslopes (mined areas are red polygons). A cross section of the gully shows that it is approximately 6.5 m deep. All gully heads measured in the White Oak watershed are shown as green points in the catchment inset map.

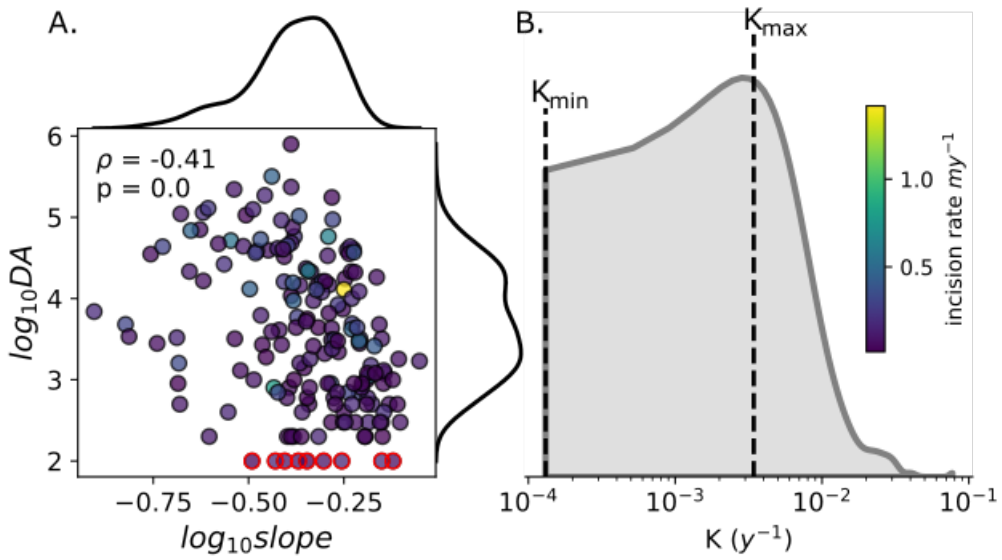

Figure 4: A) The slope and drainage area of each measured gully. A significant Spearman rank correlation suggests a monotonic relationship between slope and area, albeit with significant scatter. Points are colored by the calculated incision rate. Red outlined points were excluded from the rank correlation and K calculations because they have $A = 100$ m^2—these are DEM cells that drain only themselves. Such points arise from minor flow routing errors and are not representative of gully-forming drainage areas. B) The distribution of K calculated from erosion rate, slope and area. We take the median as the maximum K value we apply to mined portions of the landscape.

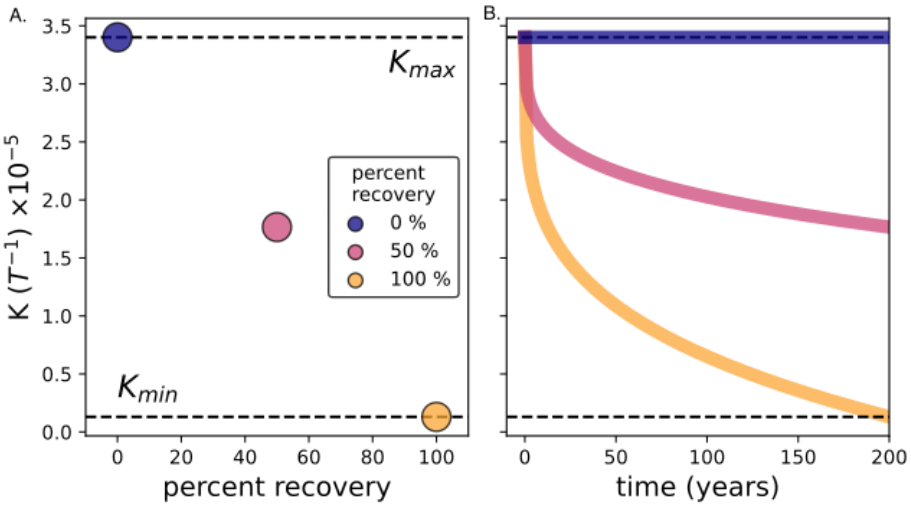

Figure 5: The three vegetation recovery scenarios. Each point represents a K^*_{min}. Right panel shows a K recovery time series for each scenario, where each scenario begins at K_{max} and recovers towards the respective K^*_{min} shown in the left panel.

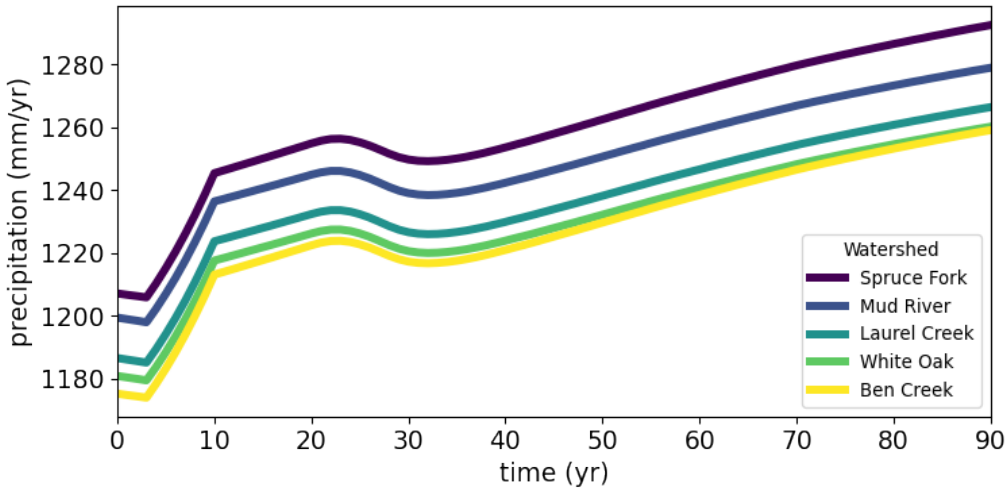

Figure 6: Mean annual precipitation projections from NASA's BioClim product (Pearson et al., 2014) averaged over each of the five study watersheds for the first 90 years of model time. Precipitation is held constant after the first 90 years.

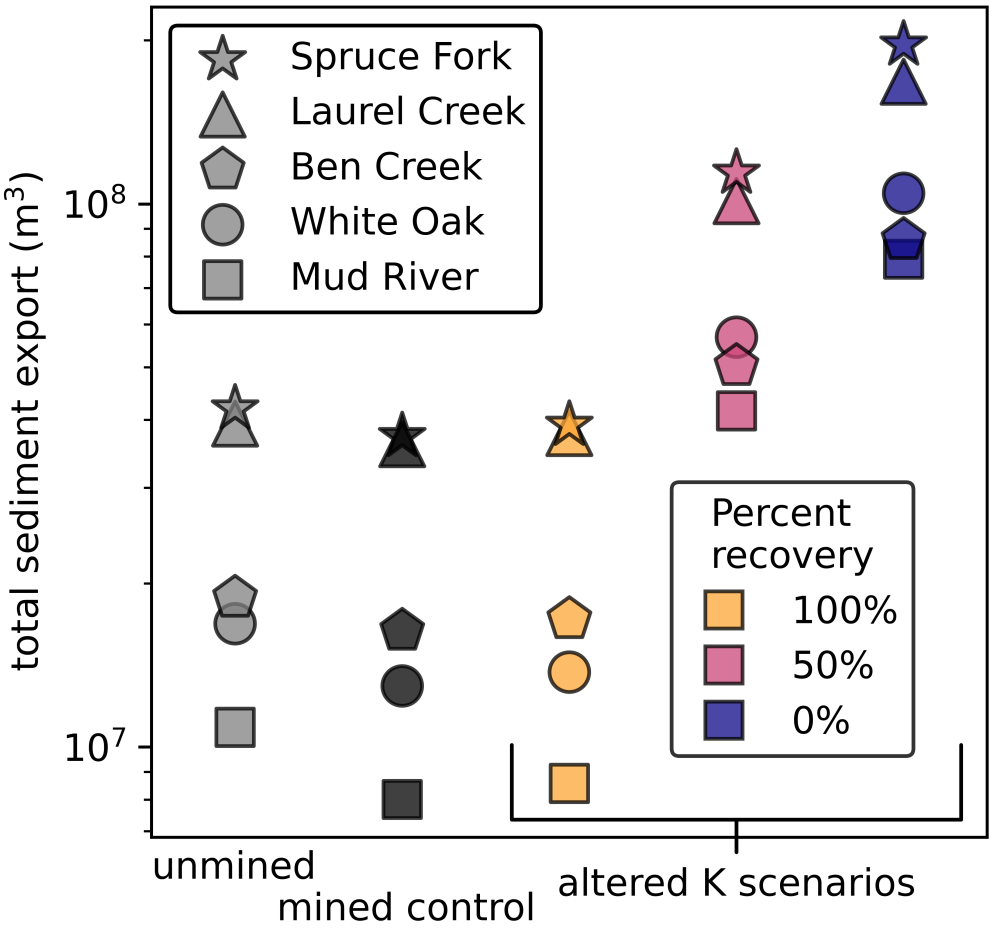

Figure 7: Total sediment export over 10 ky in each scenario. Unmined indicates simulations run using the pre-MTR DEM with no changes in erodibility; mined control indicates simulations run using the post-MTR DEM assuming no mining-induced changes in erodibility.

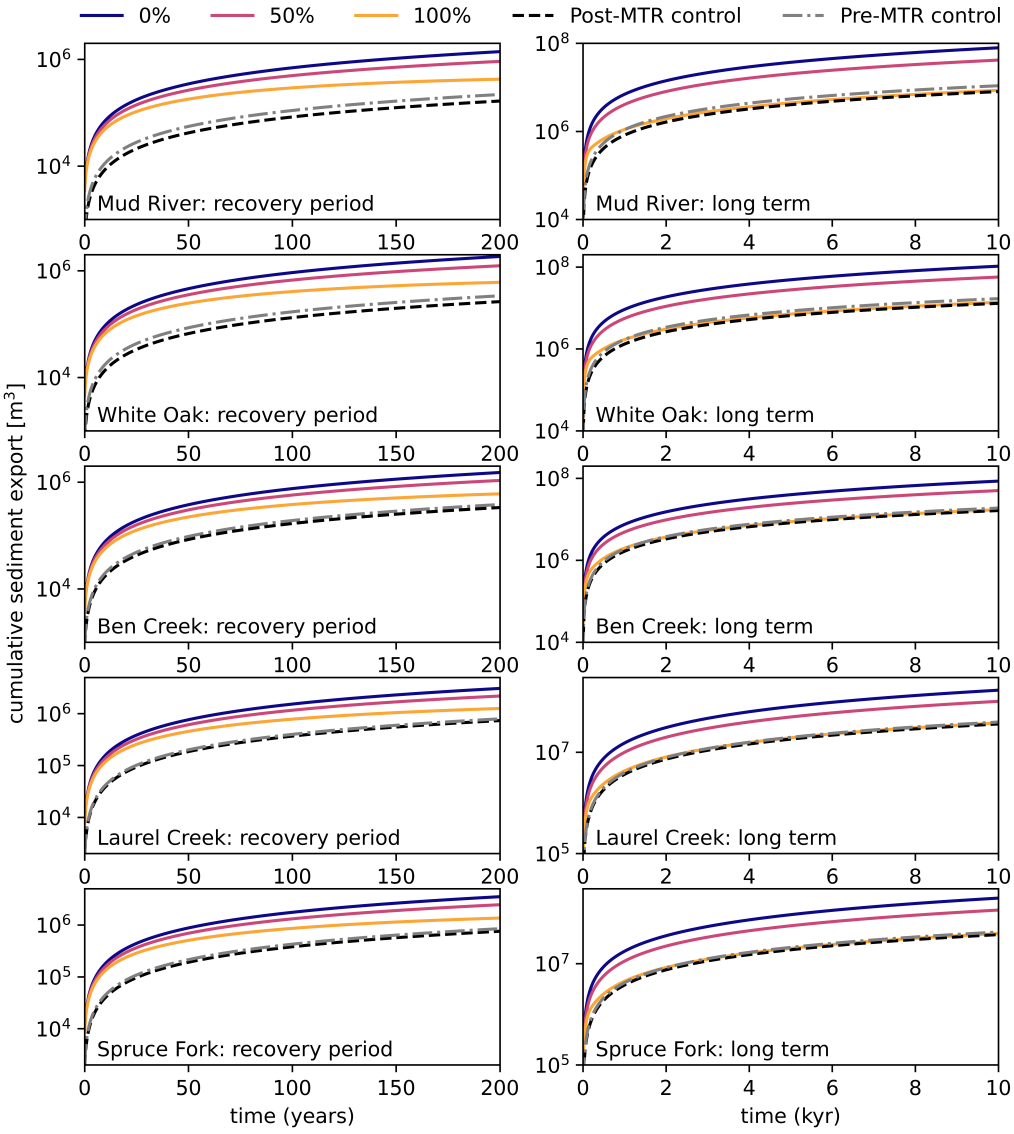

Figure 8: Cumulative sediment export for all five study watersheds over the first 200 years (the vegetation recovery period; left column) and the full 10 ky of model time (right column).

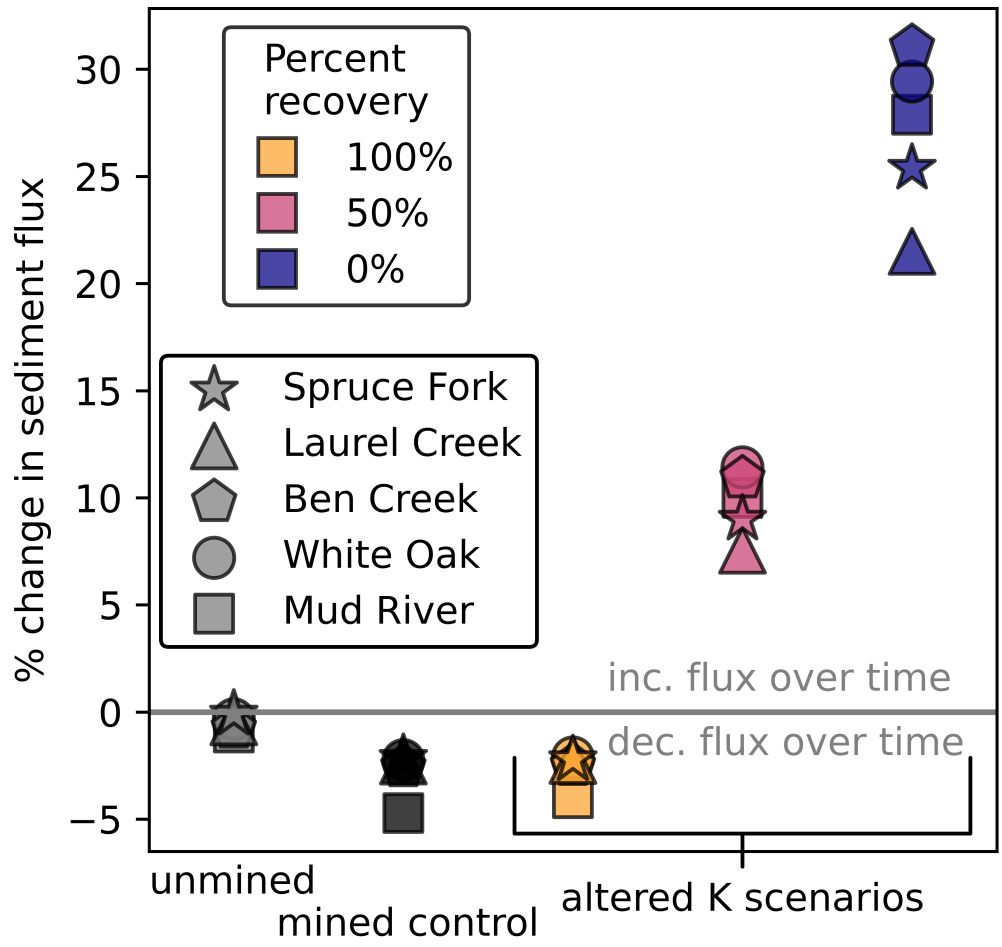

Figure 9: Percent change between sediment flux at year 200 and year 10,000. Unmined indicates simulations run using the pre-MTR DEM with no changes in erodibility; mined control indicates simulations run using the post-MTR DEM assuming no mining-induced changes in erodibility. There exists a threshold between 100% and 50% recovery governing whether MTR sets the landscape on a trajectory of increasing or decreasing sediment fluxes over time.

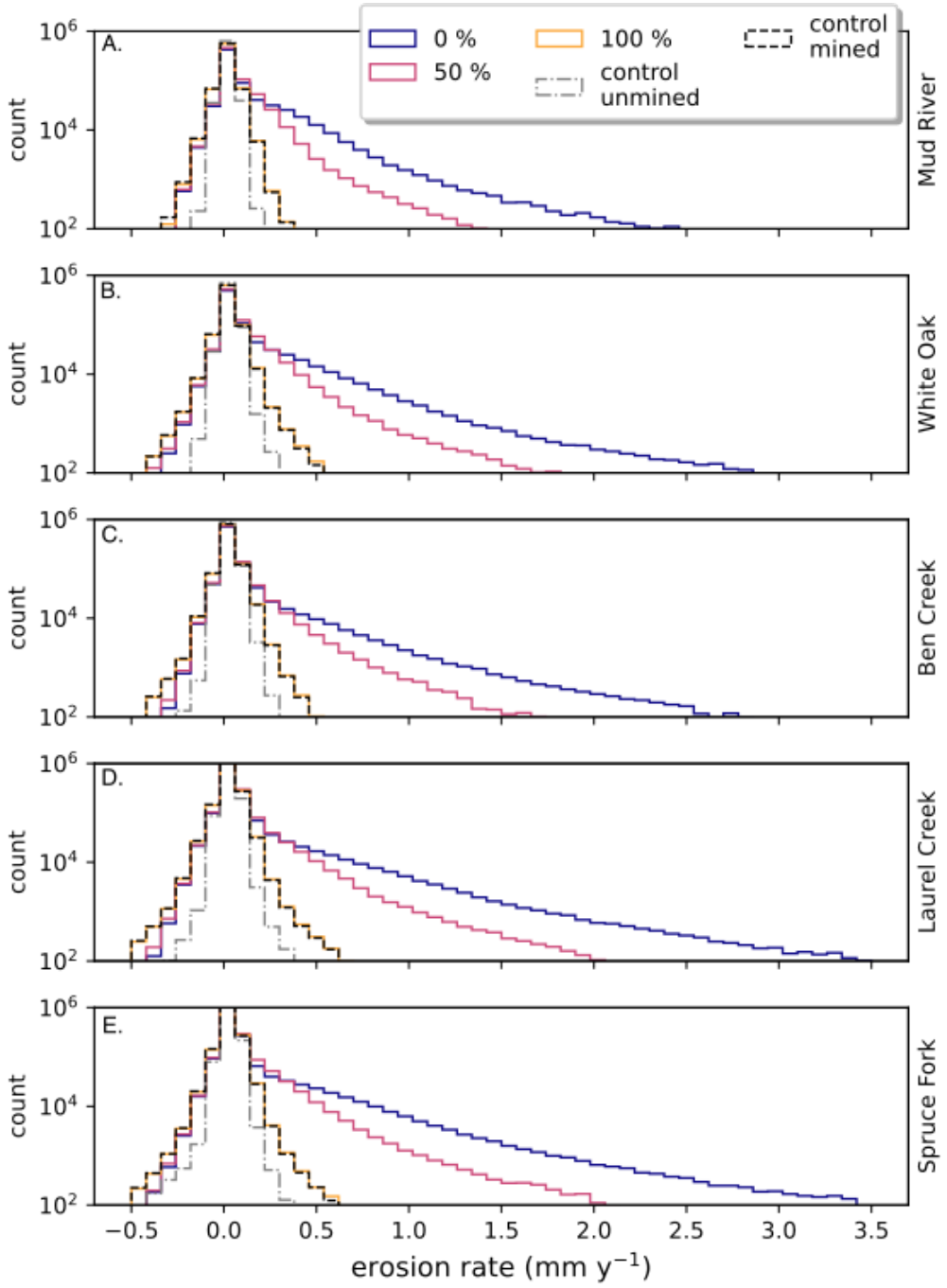

Figure 10: Distributions of erosion rates averaged over 10 kyr for all five catchments. Percentages refer to the vegetation recovery scenarios: 0%, 50%, or 100% recovery.

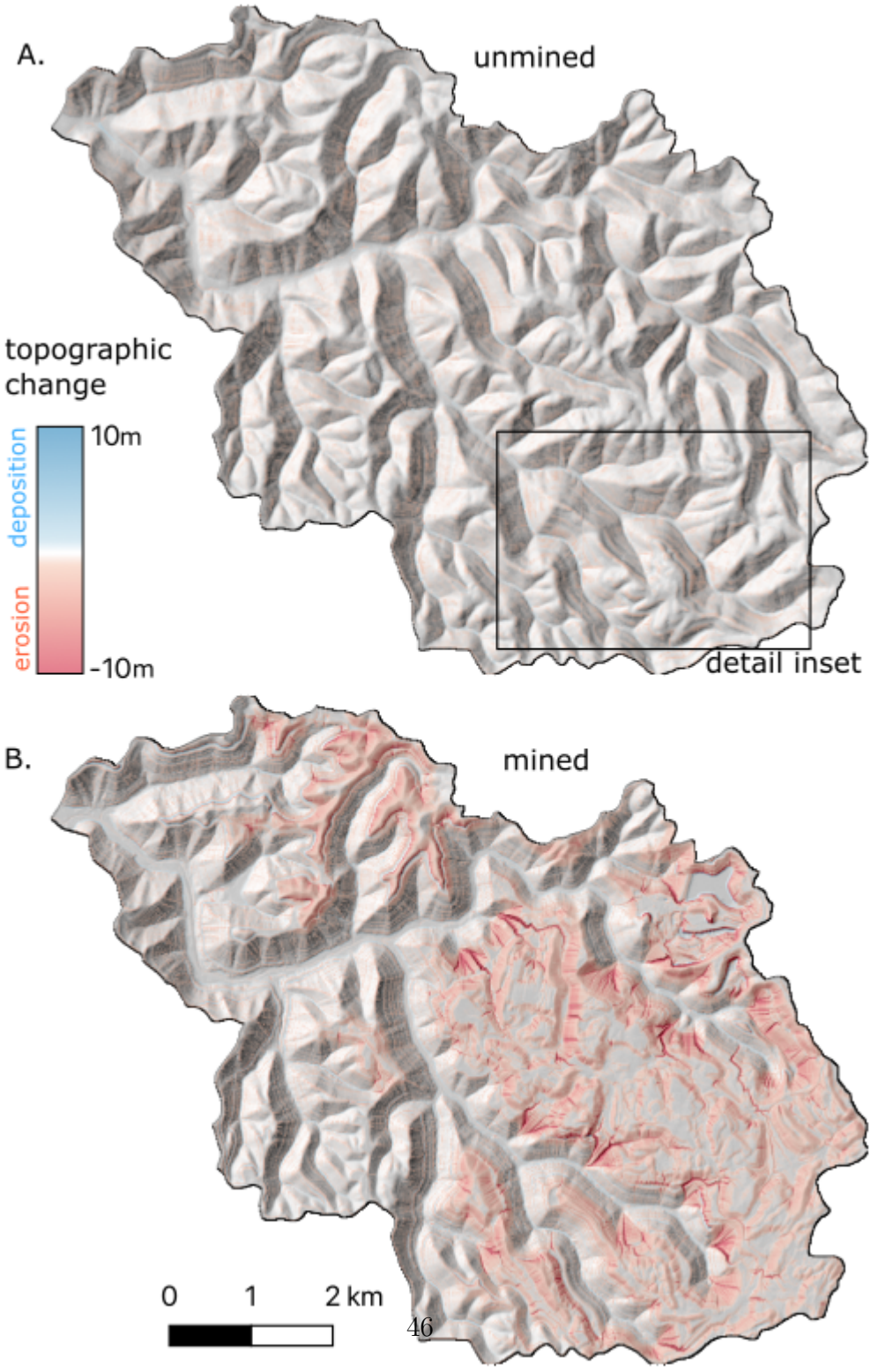

Figure 11: A) DEM of difference over 10 kyr from the White oak catchment for the 50% vegetation recovery scenario. Color bar is scaled for visual clarity; maximum erosion and deposition are -75.8 m and 7.4 m, respectively. Box shows extent of Fig. 12

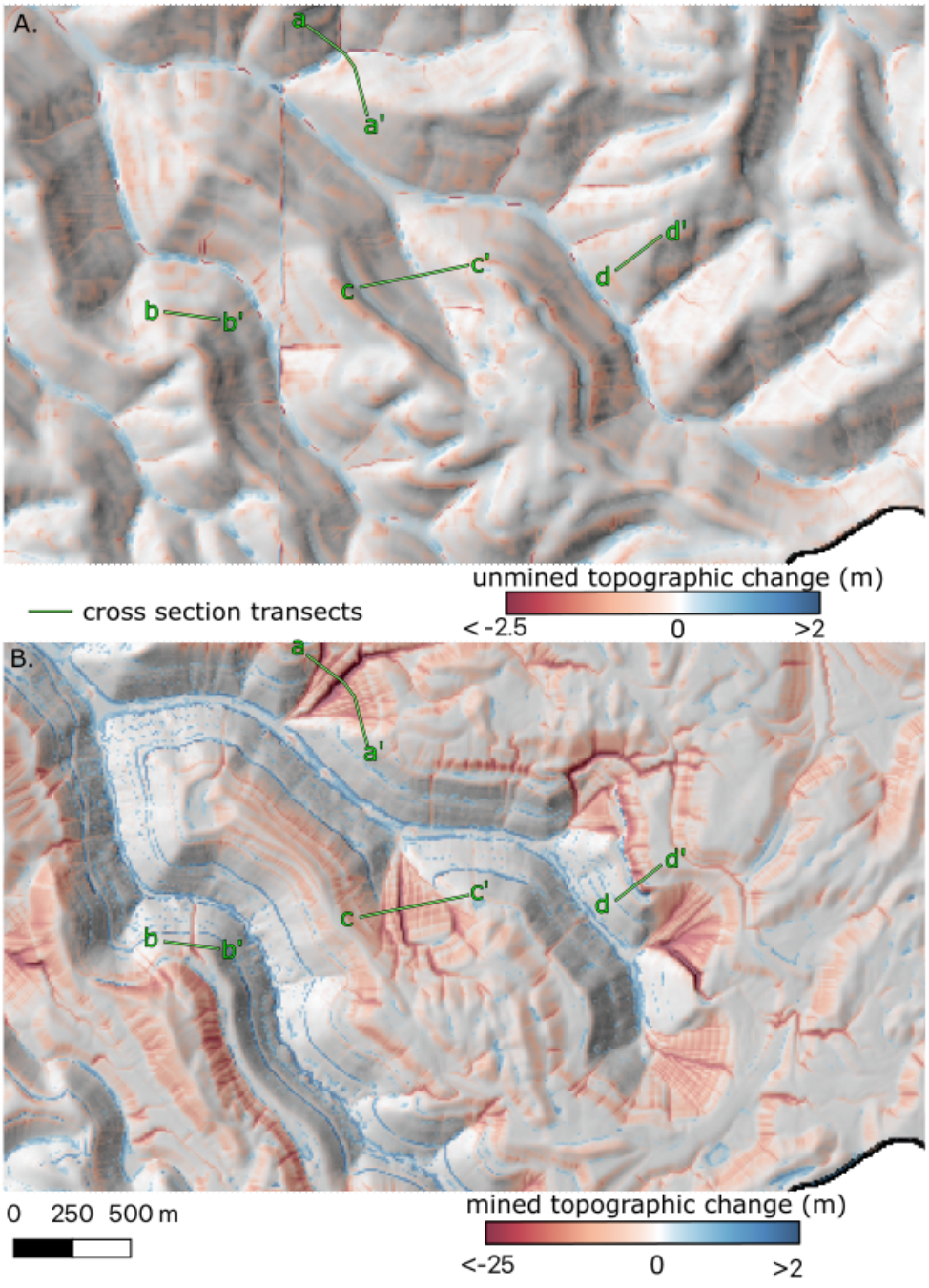

Figure 12: Selected comparisons between pre-MTR (A) simulations and post-MTR (B) simulations with 50% vegetation recovery. Both panels share the same extent, shown by the bounding box in Fig. 11. Note that a different color scale is applied to each panel. The transects in each panel show the locations of cross-sections in Fig. 13. The along-contour banding in (A) reflects artefacts from the digitization of contour line topographic maps, resulting in spurious bands of predicted erosion.

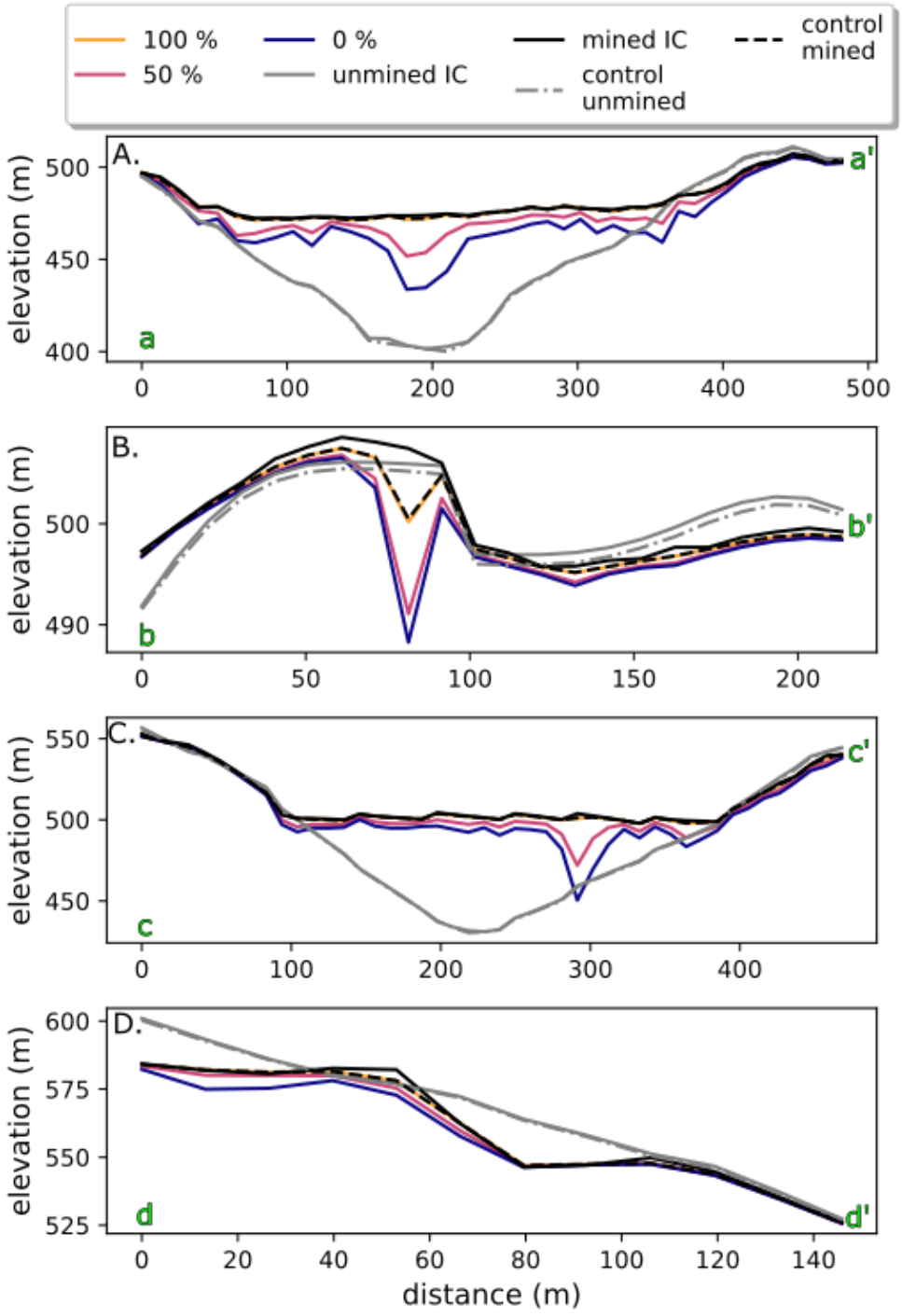

Figure 13: Cross sections corresponding to locations in Fig. 12. Cross-sections represent key landforms: A) and C) valley fill faces, B) mine-adjacent hillslope, and D) mine-related scarp.